Remote Sensing of Environment 275 (2022) 113023

Contents lists available at ScienceDirect

Remote Sensing of Environment

journal homepage: www.elsevier.com/locate/rse

Characterizing seasonal variation in foliar biochemistry with airborne imaging spectroscopy

Adam Chlus *, Philip A. Townsend

Department of Forest and Wildlife Ecology, University of Wisconsin, Madison, WI, USA

ARTICLE INFO

Editor: Jing M. Chen

Keywords:
Foliar biochemistry
Imaging spectroscopy
PLSR
Phenology
Forest

ABSTRACT

Foliar biochemical traits are important indicators of ecosystem functioning and health that are impractical to characterize at large spatial and temporal scales using traditional measurements. However, comprehensive inventories of foliar traits are important for understanding ecosystem responses to anthropogenic and natural disturbances, as inputs into ecosystem process models, and for quantifying spatial variation in functional diversity. Imaging spectroscopy has been demonstrated as a valuable tool for developing maps of ecologically important foliar traits at large scales, but its application to mapping foliar traits over the course of the growing season has been limited. We collected high-resolution imaging spectroscopy data over Blackhawk Island, Wisconsin, USA at eight time points during the 2018 growing season (May – October). Using partial least squares regression (PLSR) we developed predictive models applicable to all dates to produce canopy-level maps of eight traits related to ecophysiological function: chlorophyll content, leaf mass per area and concentrations of calcium, nitrogen, phosphorus, potassium, phenolics and lignin. The accuracy of our models varied across traits (R^2: 0.25–0.86); traits with well-defined absorption features were retrieved with high accuracy including chlorophyll (R^2: 0.86; %RMSE: 11.0) and total phenolics (R^2: 0.86; %RMSE: 11.0). We also assessed how well our models estimated biochemistry on novel species and new dates using a cross-validation analysis. Chlorophyll and total phenolics were well estimated across withheld dates and species, whereas calcium was estimated poorly on both withheld species (R^2: 0.08) and dates (R^2: 0.07). Our canopy-level maps of macronutrients (N, P and K) showed general trends of decreasing concentration over the course of the year, reflecting dilution by carbon-rich compounds during the growing season and resorption during senescence. Conversely, recalcitrant compounds including lignin and calcium increased until late summer, after which they stabilized. These results demonstrate the potential of current and proposed spaceborne imaging spectroscopy missions for mapping seasonal patterns in foliar biochemistry at a global scale.

1. Introduction

Foliar biochemical traits are dynamic properties of plants that vary through space and time and are linked to multiple ecosystem processes, including primary productivity and nutrient cycling (de Bello et al., 2010). Foliar traits include biochemical properties related to photosynthesis, such as chlorophyll and nitrogen, structure and decomposition, including fiber and lignin, and defense, like condensed tannins and other phenolic compounds. Understanding how functional traits vary through space and time is important for developing accurate ecosystem process models, for predicting ecosystem response to change and understanding patterns in community assembly (Ito et al., 2006; Reichstein et al., 2014). In general, studies that use functional traits to assess patterns in community composition and ecological function make use of mean trait values for species (Albert et al., 2011). However, variability in functional traits is known to be scale dependent and driven by both taxonomic and environmental factors (Albert et al., 2010; Messier et al., 2010, 2017). Moreover, ecosystems with strong seasonal patterns, like temperate deciduous forests, display significant variation in foliar traits as leaves develop and senesce; this variation in turn drives intra-annual patterns in ecosystem processes (Reich et al., 1991; Salminen et al., 2004; Noda et al., 2015).

Studies dating to the early 20th century reported the seasonal variation in foliar biochemical traits and demonstrated that interannual patterns vary between species, within species, and across locations (McHargue and Roy, 1932; Alway et al., 1934; Sampson and Samisch,

* Corresponding author at: Department of Forest and Wildlife Ecology, University of Wisconsin-Madison, 1630 Linden Drive, Madison WI 53706, USA.
E-mail address: chlus@wisc.edu (A. Chlus).

https://doi.org/10.1016/j.rse.2022.113023
Received 22 November 2021; Received in revised form 9 March 2022; Accepted 26 March 2022
Available online 6 April 2022

1935; Chandler, 1939). In a review of more than 20 studies, Turner et al. (1977) found that the direction of intra-annual trends (increasing, decreasing or stable) in foliar nutrient concentrations was not universal. In general, with elemental concentrations, calcium and manganese increase during the growing season, while nitrogen, phosphorus and potassium decrease, and boron, copper and magnesium are stable throughout the year. Other studies have reported on seasonal patterns in more complex compounds including pigments (Schertz, 1929; Sanger, 1971), phenolics (Schultz et al., 1982; Salminen et al., 2004; Zehnder et al., 2009), nonstructural carbohydrates (McLaughlin et al., 1980; Flower, 2007) and lignin (Martin and Aber, 1997; Zehnder et al., 2009). In general, inter- and intra-species seasonal patterns of trait variation represent trade-offs in allocation of resources, with overall trends driven by a combination of resource availability, environmental cues, species identity, phylogeny and genetics.

Trait-based ecology has emerged due the relative ease with which functional traits can be measured compared to their underlying physiological processes. This has led to the development of trait databases such as TRY (Kattge et al., 2020), which have enabled global-scale analyses of the variation in and drivers of ecosystem function (Díaz et al., 2015; Dong et al., 2020). Despite their relative ease of measurement, there are limits to the density of measurements, spatial extent and temporal richness at which functional traits can be quantified using in-situ sampling and laboratory analysis before efforts become prohibitively costly. Leaf-level spectroscopy represents a viable alternative for rapidly and nondestructively measuring foliar functional traits (Asner and Martin, 2011; Serbin et al., 2014, 2019; Couture et al., 2016), which in turn has vastly increased the amount of data available to characterize evolutionary, taxonomic and environmental sources of trait variation (Asner et al., 2014; Nunes et al., 2017; Meireles et al., 2020). Imaging spectroscopy has now also emerged as a valuable technology for further expanding the scale at which foliar functional traits can be measured. By developing relationships between canopy spectra and field measured leaf traits, maps of these traits can be generated at large spatial scales. These maps have been used to characterize relationships between canopy traits and precipitation (Asner et al., 2005), geomorphology (Chadwick and Asner, 2016a), soil chemistry (Chadwick and Asner, 2018), and land use (Swinfield et al., 2019). However, most studies using imaging spectroscopy to map foliar traits have largely focused on a single point in time, namely the peak of the growing season (Martin and Aber, 1997; Asner et al., 2015; Singh et al., 2015; Wang et al., 2020), whereas foliar traits are known to vary throughout the course of the growing season and are most dynamic during shoulder seasons following leaf out and over the course of senescence (Reich et al., 1991; Yang et al., 2016).

Remote sensing of phenology has historically been studied within the context of greenness using the normalized difference vegetation index (NDVI), or similar indices like the enhanced vegetation index (EVI), as metrics of vegetative vigor (Duchemin et al., 1999). Greenness indices are valuable for representing large-scale phenological patterns due their ease of computation and compatibility with a wide variety of remote sensing platforms (e.g., Landsat, MODIS, Sentinel). However, these indices are largely capturing variation in pigment content and leaf/canopy structure, whereas other ecologically relevant foliar traits may not exhibit the same temporal patterns (Wu et al., 2009). With its high spectral resolution, full-range (400–2500 nm) imaging spectroscopy provides the ability to resolve narrowband absorption features associated with biochemical traits not discernible from broadband sensors (Curran, 1989). Few studies have used imaging spectroscopy to study phenological patterns of foliar biochemistry of natural ecosystems (Matson et al., 1994), mostly due to lack of data. At the leaf and plant level, trait-spectra relationships vary across the course of the growing season, and predictive models developed using data from one time point may introduce biases in prediction on a different point in the growing season (Sanches et al., 2013; Yang et al., 2016). This is expected to transfer to the canopy level, but the magnitude of the effect remains untested.

Here we demonstrate for the first time the application of imaging spectroscopy to track changes in foliar biochemistry across a growing season in a temperate deciduous forest and demonstrate the ability to capture interspecific variation in biochemical phenology. Using data from eight airborne imaging spectroscopy acquisitions over Blackhawk Island, Wisconsin, USA in 2018 combined with field data, we map variation in eight canopy traits related to growth (chlorophyll, nitrogen), structure (LMA, lignin), defense (total phenolics) and mineral acquisition (calcium, phosphorus and potassium). We also assessed the capacity to estimate intraspecific variation in foliar traits and tested how well models transfer to new dates and novel species. Finally, we apply our models to the entire time series of imagery and characterize the spatiotemporal patterns in canopy biochemistry across the course of the growing season.

2. Methods

2.1. Study area

Blackhawk Island is a 73-ha island located in the Wisconsin River near Wisconsin Dells, WI, USA (43.65° N, 89.79° W) (Fig. 1). Blackhawk Island has a long history of ecological research, including some of the earliest studies linking decomposition processes, species composition and primary productivity (Pastor et al., 1984). The island has variable topography, with steep slopes along the river edge and relatively flat terrain in the center of the island, at its highest point it rises 33 m above the river. Five soil orders are present on the island, including Alfisols, Entisols, Incepticols, Histosols and Spodosols (Pastor et al., 1984). Forest community composition on Blackhawk Island is closely related to soil properties (Pastor et al., 1982). Canopy dominant species are primarily oaks (*Quercus alba and Quercus rubra*), pines (*Pinus resinosa and Pinus strobus*), and maples (*Acer rubrum and Acer saccharum*). Aboveground production is driven by soil texture and N mineralization, with mineralization rates a function of N and P return to the soil in leaf litter and litter quality variation due to species identity (Pastor et al., 1982, 1984). As a consequence of these and other studies, Blackhawk Island has also been the site of numerous studies that have used imaging spectroscopy to map canopy biochemistry (Martin and Aber, 1997; Singh et al., 2015) and is the site where Wessman and colleagues first demonstrated the potential for hyperspectral imagery to map ecosystem-relevant foliar traits (Wessman et al., 1988), especially as drivers of decomposition

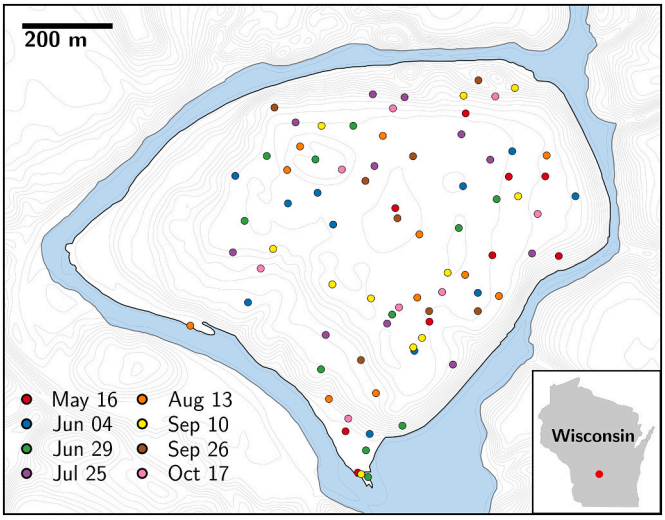

Fig. 1. Locations of sampled trees on Blackhawk Island. The western end of the island is dominated by coniferous tree species which were not included in this study.

processes.

2.2. Remote sensing data

Imaging spectroscopy data was collected using a HySpex airborne imaging system (Norsk Elektro Optikk As, Skedsmokorset, Norway). The system consists of two cameras, a VNIR-1800 camera, which measures radiation between 400 and 997 nm across 186 channels with a spectral sampling interval of 3.26 nm, and a SWIR-384 camera, which covers 975–2500 nm and measures radiation at 288 channels with a spectral sampling interval of 5.45 nm. The cameras were mounted on a vibration-dampening platform with an iTraceRT F400-E GPS/IMU (iMAR Navigation GmbH, St. Ingbert, Germany). The imaging system was flown aboard a Cessna 180 at a nominal altitude of 700 m above ground level, resulting in a spatial resolution of 0.5 m for the VNIR camera and 1.0 m for the SWIR camera. Each overflight consisted of nine flightlines with 60% sidelap. A total of eight overflights were flown between 16 May and 17 October 2018, and all flights were conducted +/− 2 h of solar noon (Table 1).

Raw image data were converted to radiance using manufacturer-provided calibration coefficients. Wavelength centers were estimated following Guanter et al. (2009). Camera alignment and geometric registration were performed using PARGE 6.0 orthorectification software (RESE, Wil SG, Switzerland). A secondary geometric adjustment was performed using a correlation-based image matching algorithm (Gao et al., 2009), using a 2015 National Agriculture Imagery Program aerial image as a reference image. Calculation of apparent surface reflectance from at-sensor radiance was performed using an inverse algebraic atmospheric correction algorithm with the 'libRadtran' radiative transfer code (Emde et al., 2016) based on the method of Adler-Golden et al. (1999). Total column water vapor was estimated using the depth of the water vapor feature at 940 nm (Carrere and Conel, 1993). Visibility, which was high during all overflights, was set to a constant of 50 km. Next, a bidirectional reflectance distribution function (BRDF) correction was applied to remove brightness gradients resulting from varying sun and sensor geometry using the approach described in Chlus et al. (2020). Briefly, using sensor and sun geometry, we modeled the volumetric, geometric and isometric scattering components using the Ross and Li scattering kernels (Schläpfer et al., 2014). For each date we pooled data across all flightlines and generated a single set of BRDF correction coefficients by regressing the resulting kernels against the uncorrected reflectance data for each wavelength. The VNIR imagery was aggregated and averaged to 1 m to match the spatial resolution of the SWIR camera. Image data from both cameras were combined at 980 nm to create a single full range (400–2500 nm) image for each flightline. The SWIR spectrum tail (>2400 nm) and water absorption bands were excluded from analysis due to low signal-to-noise ratio (SNR). Individual flightlines were merged to create a mosaic of the island for each date; in overlapping regions the pixel with the smallest viewing zenith angle (i.e., closest to nadir) was used (Fig. 2). To improve SNR we averaged bands pairwise, resulting in a total of 187 bands with nominal spectral sampling intervals of 7 nm and 10 nm in the VNIR and SWIR, respectively. Finally, to suppress residuals in the reflectance spectra we calculated per-date multiplicative correction factors, using a sand bar as a smooth reference surface (Thompson et al., 2015).

Table 1
Airborne HySpex imagery used in the study.

Overflight date	Mean local acquisition time	Local solar noon	Mean solar zenith angle
May 16, 2018	12:22	12:55	25°
June 04, 2018	11:19	12:57	29°
June 29, 2018	12:18	13:02	22°
July 25, 2018	13:38	13:05	25°
August 13, 2018	14:26	13:04	34°
September 10, 2018	12:18	12:56	39°
September 26, 2018	12:40	12:50	45°
October 17, 2018	12:22	12:44	53°

2.3. Foliar sampling

Within eight days of each overflight, we collected foliage from 9 to 11 trees. To ensure that our field-derived foliar measurements were from trees identifiable in the imagery we sampled trees that had crowns greater than 5 m in diameter. From each tree we sampled 1–3 branches from the sun exposed top of the canopy. Branches were sampled using either extendable pole pruners or a custom-built cutting device (Chlus et al., 2020). From each branch we measured the reflectance of 20 leaves with a PSR 3500+ spectrometer equipped with a leaf clip (Spectral Evolution, Boston, MA, USA) to estimate leaf-level foliar traits using spectroscopic models. Of those 20 leaves, we measured the one-sided area of three leaves using a flatbed scanner to calculate leaf mass per area (LMA) and retained a single leaf for pigment analysis to validate the spectral models. We combined the remaining 16 leaves with an additional 20–30 leaves from each branch for bulk chemical analyses. All foliar samples were stored in plastic bags with a damp paper towel in coolers with ice until the end of each day when they were frozen in liquid nitrogen and stored in a − 20 °C freezer until further processing. In addition to foliar sampling, we also recorded the species, diameter at breast height (DBH), crown shape of each tree sampled and made a general site characterization. We recorded tree locations with a differentially corrected GeoXM or Geo7x GPS receiver (Trimble Inc., Sunnyvale, CA, USA). Over the course of the study period a total of 80 trees were sampled representing 11 broadleaf species (Table S1).

2.4. Sample processing

Bulk foliar samples were dried in a lyophilizer (> 120 h) and ground using a Wiley Mill (Thomas Scientific, Swedesboro, NJ, USA) equipped with a #20 mesh (0.841 mm). A subset of ground samples was analyzed for concentrations of elements (N, P, K, Ca) ($n = 27$), total phenolics ($n = 49$) and acid-digested lignin ($n = 28$). Elemental concentration was determined using combustion analysis (N) and inductively coupled plasma emission spectroscopy (Ca, K, P) (Gavlak et al., 2003). Total phenolics concentration was determined using the Folin-Ciocalteu method (Ainsworth and Gillespie, 2007), while lignin concentration was determined using a hot-acid detergent extraction (Couture et al., 2012). Leaves measured for leaf area were dried for >72 h in a 68 °C oven and weighed on a precision balance (0.0001 g) to determine dry mass. LMA was calculated by dividing measured dry mass by leaf area. Chlorophyll A content was measured on a subset of samples ($n = 63$) using high performance liquid chromatography (HPLC) following Schweiger et al. (2018).

Spectral measurements were made on all dried and ground samples with an ASD Fieldspec 3 spectrometer (Analytical Spectral Devices, Boulder, CO, USA) following Serbin et al. (2014). Prior to spectral measurements ground samples were stored in a 68° oven overnight to remove any residual moisture absorbed during storage. Spectroscopic models were then used to estimate foliar biochemistry for all samples. Estimation of foliar traits from reflectance spectra is a well-established method for rapidly and accurately estimating foliar biochemical properties (Asner and Martin, 2008; Serbin et al., 2014; Yang et al., 2016). Fresh leaf-level reflectance spectra were used to estimate LMA and chlorophyll A content, while spectra of dried and ground samples were used for the estimation of all other traits. Models were built using partial least squares regression (PLSR) using 'scikit-learn' in Python (Pedregosa et al., 2011). PLSR models were calibrated with data from three independent datasets: Serbin et al. (2014), Wang et al. (2020) and Chlus et al. (*In prep.*) and validated against the subset of samples from Blackhawk Island that were measured using laboratory techniques. Models for

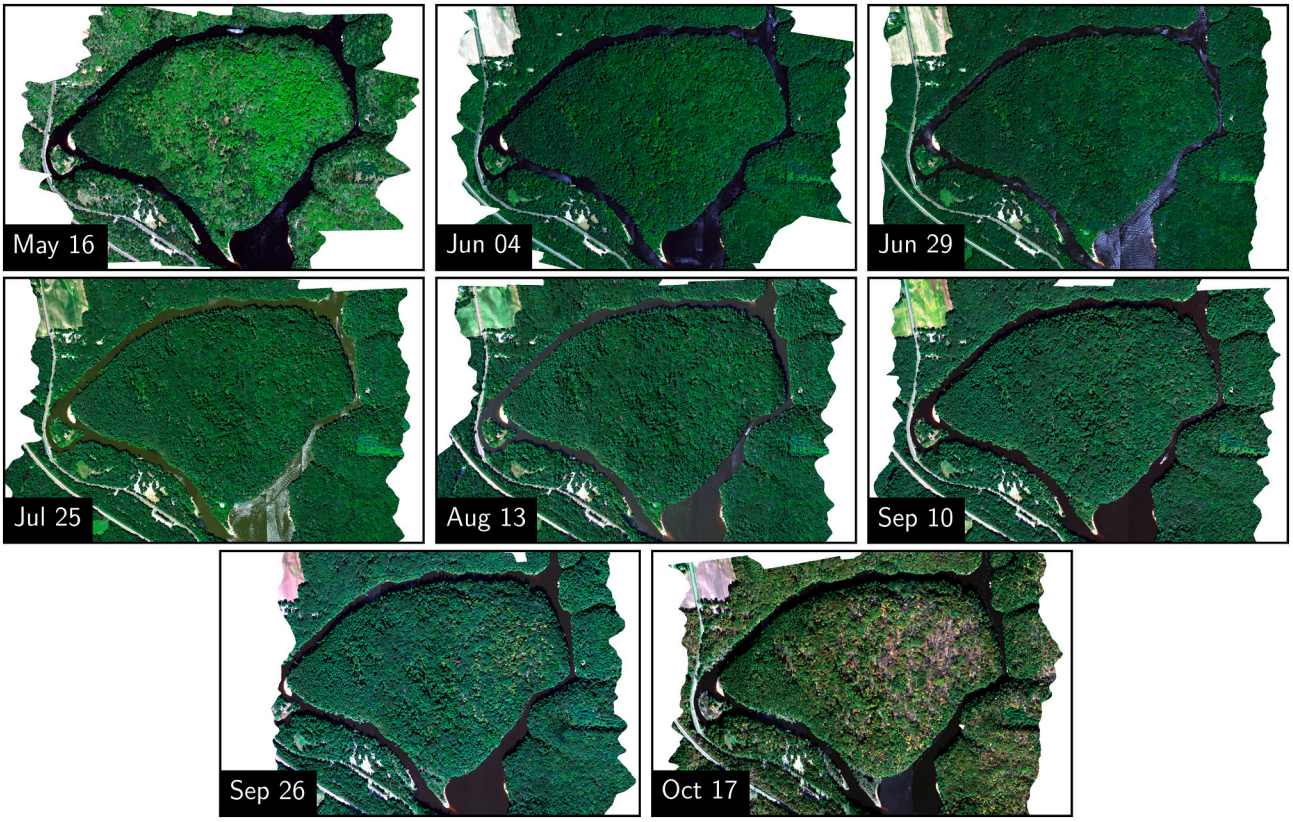

Fig. 2. True color RGB mosaics of HySpex imagery for each overflight date.

all traits were built using the SWIR region of the spectrum (1200–2500 nm), with the exception of chlorophyll A models that used the VNIR (400–750 nm). Prior to model building, each spectrum was normalized to its mean to remove brightness differences, similar to normalization used in other studies (Feilhauer et al., 2010; Kim et al., 2013). The optimal number of model components was determined using the cross-validated predicted residual sum of squares (PRESS) calculated on the calibration dataset. A series of 500 calibration models was generated, each built using a random 70% of the calibration data. These models were then applied to the independent (fully withheld) validation dataset and the mean trait value across the 500 models was calculated for each sample and compared against the observed trait value. Model performance was assessed using the coefficient of determination (R^2), root mean squared error (RMSE) and normalized RMSE (%RMSE) (Table S2). Following the accuracy assessment, 500 new permuted models were built using the entire dataset and were applied to all fresh and ground spectra. Any negative trait predictions were truncated to zero.

2.5. Canopy trait mapping

Trait maps were generated using PLSR, predicting canopy-level traits as a function of HySpex imaging spectroscopy. We chose PLSR over other modeling methods due to its computational efficiency, ease of interpretation and track record for accurately estimating foliar biochemistry from imaging spectroscopy (Chadwick and Asner, 2016a, 2016b; Martin et al., 2018; Wang et al., 2020). In-situ top-of-canopy traits were derived by simple averaging of all leaf-level trait estimates from sampled branches from each tree. Canopy spectra of sampled trees were extracted from the imagery using manually digitized crown polygons and averaged, resulting in a single spectrum per tree. We used all pixels from a crown, including both sunlit and shaded components, as this is more representative of canopy spectra than using sun-facing pixels exclusively, and also better facilitates comparison with coarser-resolution data expected from forthcoming satellite missions. Similar to the leaf-level models we mean-normalized the canopy spectra prior to analysis.

For each trait we began by randomly dividing the data 70:30 for calibration and validation. The optimal number of model components was determined by minimizing the cross-validated PRESS statistic calculated on the calibration dataset, up to 20 components. Next, we built a series of 500 permuted models, each using a random 70% subset of calibration dataset. These models were applied to the original validation subset and averaged by validation sample across all permutations. To evaluate the predictive ability of the model we calculated the R^2, RMSE and %RMSE for both calibration and validation datasets. We found that due to the sample size of 80 the optimal model and model performances varied widely as a function of the original random split, leading to both under- or over-optimistic results among all of the permutations (Fig. S1). To get a better representation of model performance we repeated the model building process 500 times, each with a new random 70:30 split of the data for calibration and validation (See Fig. S2 for details). This resulted in 25,000 sets of model coefficients (500 splits $\times$ 500 permutations), to reduce the number of coefficients used for prediction each set of permuted model coefficients was averaged, resulting in a total of 500 models. The resulting 500 models were applied to all images in the time series and the mean trait estimates were calculated for each pixel. We also calculated per-pixel trait standard deviation as a measure of predictive uncertainty. For analysis, we masked pixels whose values were outside $\pm$15% of the range of field measured traits or had negative values.

To test the sensitivity of our models to both novel species and new dates we performed a leave-one-group-out cross-validation, where we withheld for validation either species or image collection dates. For each withheld group, we developed a permuted PLSR model using data from the remaining groups and applied this model to the withheld group data. Due to the small number of individual trees sampled for *Betula* species (*n*

= 2 for *Betula alleghaniensis* and $n = 3$ for *B. nigra*) data from these species was aggregated, and data from *A. sacharinum* data (n = 3) were included with *A. rubrum* ($n = 9$), a closely related species (Saeki et al., 2011). The PRESS statistic was used to select the optimal number of components, up to 20 components, for each cross-validation split. Model performance was evaluated using the R^2, RMSE and %RMSE of the out-of-sample datasets. R^2 metrics were calculated from the linear fit between the predicted and observed values while %RMSE was calculated using the full season range to allow for comparison among dates and species.

All canopy-level models were built using the SWIR region of the spectrum with the exception of chlorophyll A (400–750 nm) for which we aimed to exploit pigment absorption features (Curran, 1989; Gitelson et al., 1996). The remaining traits were predicted using only the SWIR spectrum (1200–2400 nm) because the primary absorption features associated with those traits are located in the SWIR (Curran, 1989; Workman Jr and Weyer, 2008), but also to reduce confounding influence of pigment-related spectral features in the visible that may correlate with non-pigment traits and to limit the influence of canopy structure in the NIR wavelengths.

2.6. Species classification

To assess species-specific patterns in mapped traits we developed a species map of the island. Species classification was performed using an object-oriented (segmentation) classification approach, in which both spatial context and spectral signatures are used to delineate trees. Image segmentation was performed using the Shepherd segmentation algorithm (Shepherd et al., 2019) implemented using the Python library 'RSGISLib' (Bunting et al., 2014). Shepherd segmentation uses an iterative process of grouping spectrally similar regions of pixels until all regions reach a user-defined minimum mapping size, which we established as 25 pixels (25 m^2) to correspond to the minimum crown size sampled. The segmentation was performed on a five-band composite of principal component (PC) images from three dates 16 May (PC bands: 2, 4, 5), 04 June (PC band: 4) and 29 June (PC band: 4). We used multiple dates to exploit phenological and spectral differences among canopy tree species. The PC transformation was performed to reduce the dimensionality of the data, thus improving processing time and limiting data redundancy. We visually inspected the PCs and chose for segmentation those that showed the greatest amount of contrast between neighboring crowns. Late season images were not used as testing demonstrated that they provided no improvement in segmentation results.

After segmentation, species classification was performed using a bootstrapped random forest classifier built with 100 trees using the 'scikit-learn' library in Python (Pedregosa et al., 2011). For each segment we calculated the mean value of all contained pixels for each band across seven dates, resulting in 1309 features per segment (187 bands × 7 dates). Imagery from October 17 was excluded due to asynchronous senescence of deciduous species across the island. To reduce the dimensionality of the data we applied a PC transformation and retained as predictor variables the first 78 components, which explained >99.99% of the variance in the data. Species labels for training and testing of the classifier were derived from a combination of field data collected in 2018 and 2019 and photointerpretation, yielding 418 individual trees representing 13 species. We excluded species for which there were less than three individuals found on the island, including yellow birch (*B. alleghaniensis*), cottonwood (*Populus deltoides*) and elm (*Ulmus* sp.). We used the point locations associated with the identified trees to select the corresponding image segments. The data were then split 50:50 into training and testing data, stratified by species. A classification model was built with the training dataset and used to label the testing dataset, on which we calculated accuracy metrics. After accuracy assessment the classifier was rebuilt using all of the data and applied to all image segments to make a map to intersect with the trait maps. We retained the classification probability of each segment to use in subsequent analyses to filter segments with less than 30% classification probability and eliminate canopy gaps and low growing vegetation.

3. Results

3.1. Canopy trait models

The results of the full-season PLSR models varied by trait (R^2: 0.25–0.86), and, with the exception of calcium, all traits had a %RMSE of less than 20% (Table 2). Values of standardized PLSR coefficients provide a basis for interpretation of the models, with highly negative coefficients expected to correspond to spectral absorption features. Models for estimating chlorophyll A content and total phenolics showed the strongest predictive performance (R^2: 0.86%RMSE: 11%), and both leveraged well-documented spectral features, the red edge (685–730 nm; Gitelson et al., 1996) for chlorophyll and aromatic C—H absorption (1660 nm; Kokaly and Skidmore, 2015) for total phenolics. Similarly, large negative standardized coefficients for nitrogen were present at 2050 and 2017 nm, wavelengths with absorption features associated with proteins and N—H bonds (Curran, 1989; Osborne et al., 1993). The standardized coefficients for lignin exhibited a large negative value at 1685 nm, a wavelength associated with C—H and C═O bonds in lignin (Workman Jr and Weyer, 2008). Standardized model coefficients for both phosphorus and potassium were the most similar to each other among all pairwise comparisons (Pearson r: 0.74) and both exhibited large negative coefficients at 1735 and 2215 nm (Fig. 3). Conversely, potassium and total phenolics showed the strongest negative correlation between standardized coefficients (Pearson r: −0.57) and both exhibited coefficient peaks at 1660 nm, negative for total phenolics and positive for potassium.

Similar ordering of model performances was seen in species cross-validation analyses (Fig. 4; See Table S4 for detailed metrics). Chlorophyll A content was well estimated on withheld species (R^2: 0.64–0.98) whereas calcium concentration was generally poorly estimated (R^2: 0.0–0.66). Total phenolics were systematically underestimated in *A. rubrum* and *A. saccharinum* species when withheld (Bias: −4.77% mass) compared to all other species (Bias: −1.39–2.25% mass).

The ability of our models to estimate total phenolics content on new dates was high (R^2: 0.7–0.97, %RMSE ≤ 17%; Fig. 5), whereas calcium models generally performed poorly on new dates (R^2: 0–0.9, %RMSE: 12–55%). Estimates of LMA on June 29 and September 26 exhibited a systemic underestimation of 24 and 21 g m^{-2}, respectively. We found that on average across all traits, errors were highest at the beginning (May 16, %RMSE: 19.6%) and end of the season (October 17, %RMSE: 16.9%).

3.2. Species classification

The accuracy of the classifier was high (Overall accuracy: 88.5%; Cohen's kappa: 0.87; see Table S5 for details). With the exception of white ash, all species had user's and producer's accuracies of 75% or greater. Red oak (*Quercus rubra*) was the most common tree species on Blackhawk Island (40% cover), followed by white pine (*Pinus strobus*) (17%) and sugar maple (*Acer saccharum*) (12%), with all other species having less than 10% cover.

3.3. Seasonal patterns

Species-averaged trait trajectories varied across the course of the growing season (Fig. 6). Traits associated with leaf structure, including LMA and lignin, displayed similar species ordering from low to high values on all dates, and followed a generally similar trend of increasing values until leveling off in the late summer. Calcium displayed a similar trend, but species ordering differed from LMA and lignin, with *Tilia americana* and *Carya cordiformis* accumulating the greatest concentrations of calcium among the five broadleaf species. Chlorophyll A content

Table 2
Average calibration and independent validation metrics for 500 permutations of full-season canopy-level PLSR trait model. C indicates median number of components used in the permuted PLSR models.

				Calibration				Validation			
Trait	Units	Wavelengths (nm)	C	R^2	RMSE	%RMSE	Bias	R^2	RMSE	%RMSE	Bias
Calcium	% mass	1201.4–2389.4	6	0.61	0.4	0.13	0	0.25	0.67	0.26	0.03
Chlorophyll A	μmol m^2	407.1–745.6	5	0.91	38.68	0.07	0.23	0.86	52.7	0.11	−1.03
LMA	g m^2	1201.4–2389.4	14	0.91	5.71	0.06	0.11	0.58	14.35	0.17	0.42
Lignin	% mass	1201.4–2389.4	12	0.91	1.34	0.07	0.01	0.62	2.91	0.17	−0.03
Nitrogen	% mass	1201.4–2389.4	14	0.94	0.17	0.04	0	0.67	0.42	0.15	0
Phosphorus	% mass	1201.4–2389.4	6	0.81	0.03	0.09	0	0.66	0.04	0.16	0
Potassium	% mass	1201.4–2389.4	9	0.88	0.15	0.07	0	0.63	0.31	0.17	−0.01
Total phenolics	% mass	1201.4–2389.4	10	0.96	0.9	0.05	0.01	0.86	1.75	0.11	0.06

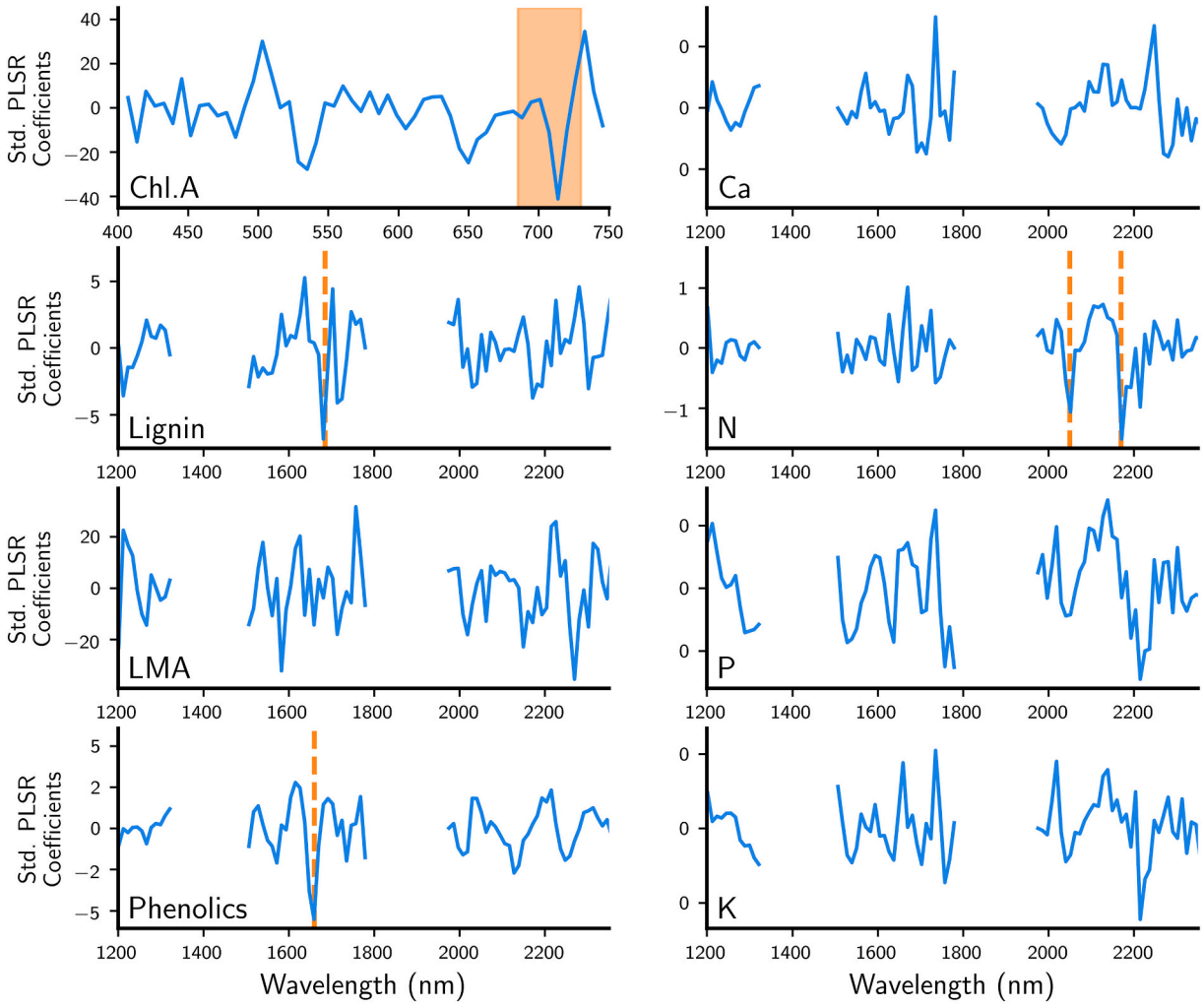

Fig. 3. Averaged full season standardized PLSR model coefficients. Dashed vertical lines and shaded regions indicate locations of reported spectral features that align with standardized coefficients (see Table S3).

trajectories showed the greatest dynamic range among all traits with a two-fold increase and subsequent decrease over the growing season. All species had similar seasonal trends but showed differences in phenological timing and, with the exception of *B. nigra,* all species had similar magnitudes of maximum chlorophyll content (> 400 μmol m^{-2}). Nitrogen, potassium and phosphorus decreased in concentration as the season progressed, but rates of decrease varied among traits and species. After full leaf expansion, nitrogen concentration was stable during the peak of the growing season before declining in late September, while phosphorus and potassium exhibited a gradual and continuous decline across the growing season. Seasonal trajectories of phenolics varied most widely across species in both magnitude and direction. *Acer* species had the highest phenolics concentration among the common species on Blackhawk Island, and gradually decreased over the course of the growing season. *C. cordiformus*, *Q. rubra* and *T. americana* displayed a U-shaped seasonal pattern, with the highest concentrations of phenolics early and late in the season.

We visualized the trait maps by generating three band composite images across four dates in the growing season and summarized the species-average patterns in the eight most common broadleaf species on the island (Fig. 7). Here we display total phenolics, LMA and potassium in the red, green and blue channels, respectively, as these traits have

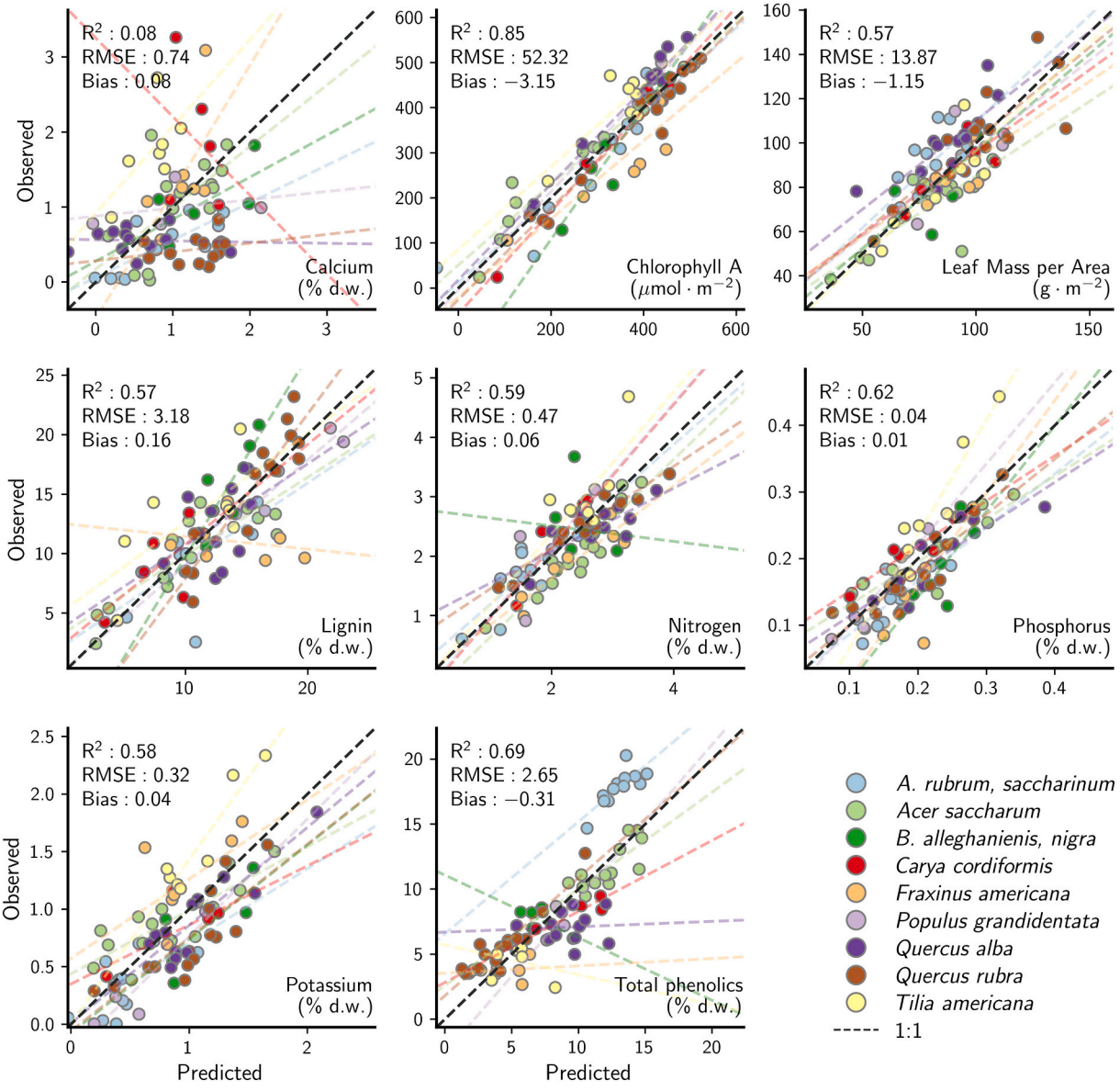

Fig. 4. Cross-validation results for species iteratively withheld from image PLSR model building. Colored lines correspond to linear fit between predicted and observed values for each species or group of species. Overall R^2 and RMSE and bias reported; metrics for individual species in Table S4.

different seasonal trajectories and show distinct patterns in species sorting (Fig. 6). For visualization, each trait value was first normalized to 10–90 percentile range across all four dates, then for each date and pixel, traits values were normalized to their sum. On May 16 broadleaf species are characterized by relatively high concentrations of total phenolics and potassium and low LMA and exhibit two distinct groupings, *Acer* species and non-*Acer* species. Beginning on June 04, non-*Acer* species begin to diverge, but generally exhibit a relative decrease in total phenolics content captured by the shift in color from purple to blue. As the season progressed, LMA increased across all species resulting in an island-wide shift towards green on the map. In the July and September composite images there is a distinct gradient in tri-variate trait space of species: from species with high phenolics, low potassium and lower LMA than other species (specifically maples) to those with comparatively high LMA and relatively lower phenolics (red oak, white oak), with basswood standing out as intermediate in LMA and phenolics but comparatively higher than other species in potassium.

4. Discussion

4.1. Cross-seasonal trait mapping

Using a time series of imaging spectroscopy data over a single growing season, we developed maps of canopy foliar traits to characterize phenological variation in a temperate broadleaf forest. We demonstrate that accurate maps of canopy traits can be derived using a single cross-seasonal model per trait and that these models accurately characterize interspecific trait trajectories (Fig. 6). Models that performed best included those with strong absorption features in the VSWIR spectrum (400–2500 nm), including chlorophyll (R^2: 0.86) and total phenolics (R^2: 0.86). Other traits, like calcium, despite lower validation R^2 (R^2: 0.25), still accurately captured interannual trends with a validation RMSE of 26% of the data range and aligned with species ordering as reported in the literature (Chandler, 1939; Chandler, 1941; Insley et al., 1981; Côté and Fyles, 1994). In addition to chlorophyll and phenolics, we also found that PLSR models for nitrogen and lignin leveraged well documented molecular absorption features (Fig. 3).

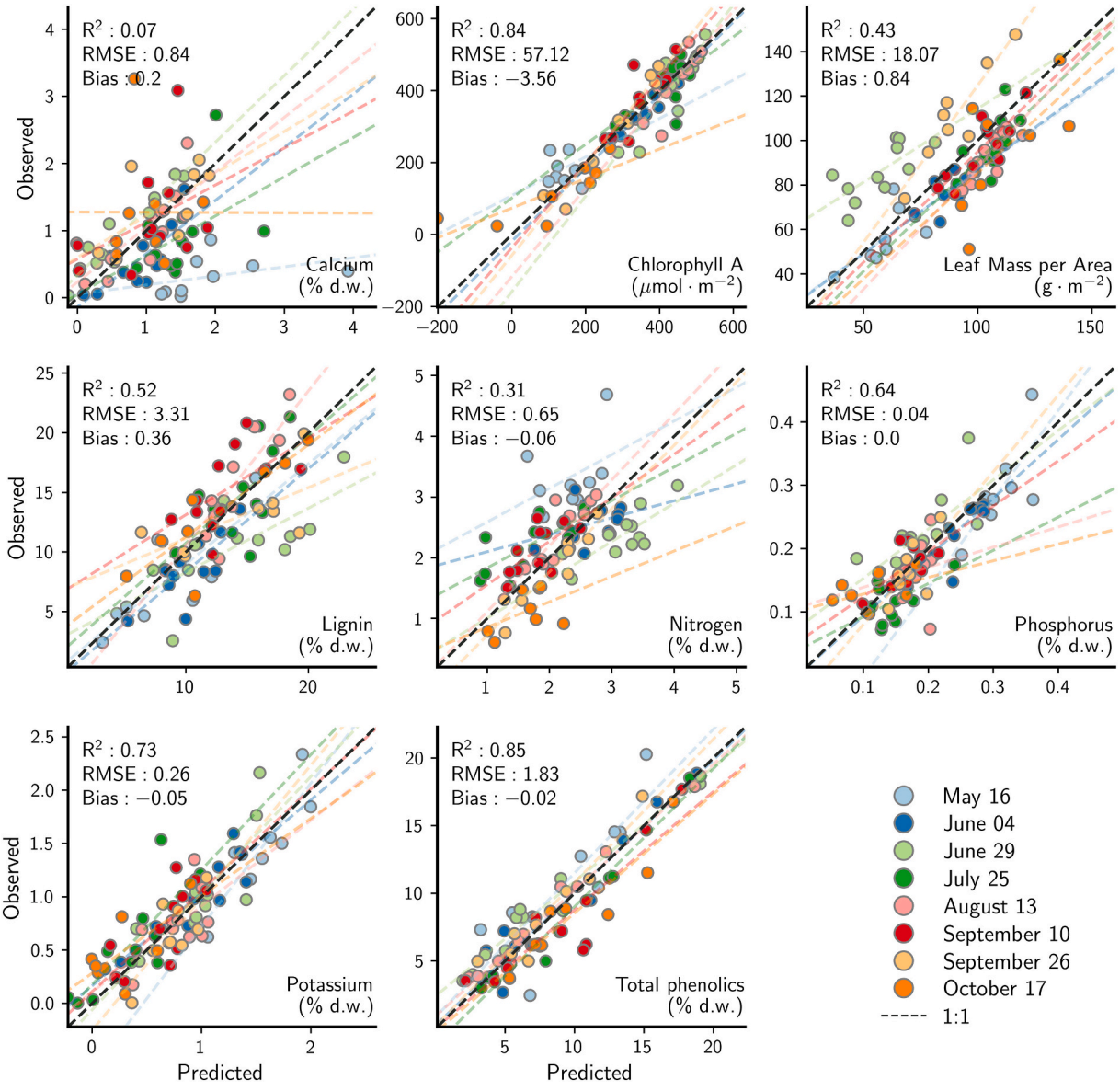

Fig. 5. Cross-validation results for dates iteratively withheld from image PLSR model building. Colored lines correspond to linear fit between predicted and observed values for each date. Overall R^2, RMSE and bias reported; metrics for individual dates in Table S5.

Other biochemical traits like potassium and phosphorus, despite having no or very weak absorption features in visible through shortwave range (Shenk et al., 1979; Workman Jr and Weyer, 2008), were well estimated, indicating the ability to accurately map these traits is due to correlations with other compounds. Coefficients for both traits were positively correlated ($r = 0.74$; $p < .001$) and showed standardized coefficient minima and maxima at 2215 nm and 1735 nm, respectively (Fig. 3). 1735 nm is a characteristic absorption band of the C—H group (Workman Jr and Weyer, 2008) and its use in accurately estimating P and K may reflect the impact of increasing concentration of carbon rich compounds on the dilution of phosphorus and potassium as leaves develop. LMA, which is a composite measure of dry mass per unit area, had standardized coefficient minima at 1582 and 2270 nm, wavelengths that are associated with absorptions by dry matter constituents including cellulose, starch and sugar (Curran, 1989). Conversely, the coefficient maximum occurred at 1758 nm, while the associated spectral absorption feature is unclear, Cheng et al. (2014) found a wavelet featured centered on 1756 nm to be correlated with LMA.

Similar to the full season analyses, models for traits with strong absorption features exhibited the strongest performance in the cross-validation analysis in which species or dates were withheld. However, our cross-validation results highlight the limitations of data-driven algorithms for predicting beyond the range of measurements on which the model was developed. For example, concentrations of total phenolics were underestimated in *A. rubrum* and *A. saccharinum*, species with high concentrations of phenolics, when applying models calibrated using datasets in which maples were excluded. Unlike leaf-level spectroscopy, which allows for the collection of reflectance measurements under controlled conditions (i.e. leaf clip or integrating sphere), imaging spectroscopy presents multiple additional challenges for trait estimation based on canopy reflectance retrievals. These include radiometric calibration, atmospheric correction and BRDF correction (Weyermann et al., 2013; Thompson et al., 2018), as well as other factors such as crown architecture, canopy openness and the presence and relative density of understory vegetation. These impacts can be seen in our cross-validation results (Fig. 5) and seasonal trajectories (Fig. 6): on some dates trait retrievals appear systematically biased across all species (e.g., see June 29 for LMA and nitrogen). However, these biases are not universal across traits and are likely a function of both model wavelength weightings (Fig. 3) and crown characteristics. For example, we found

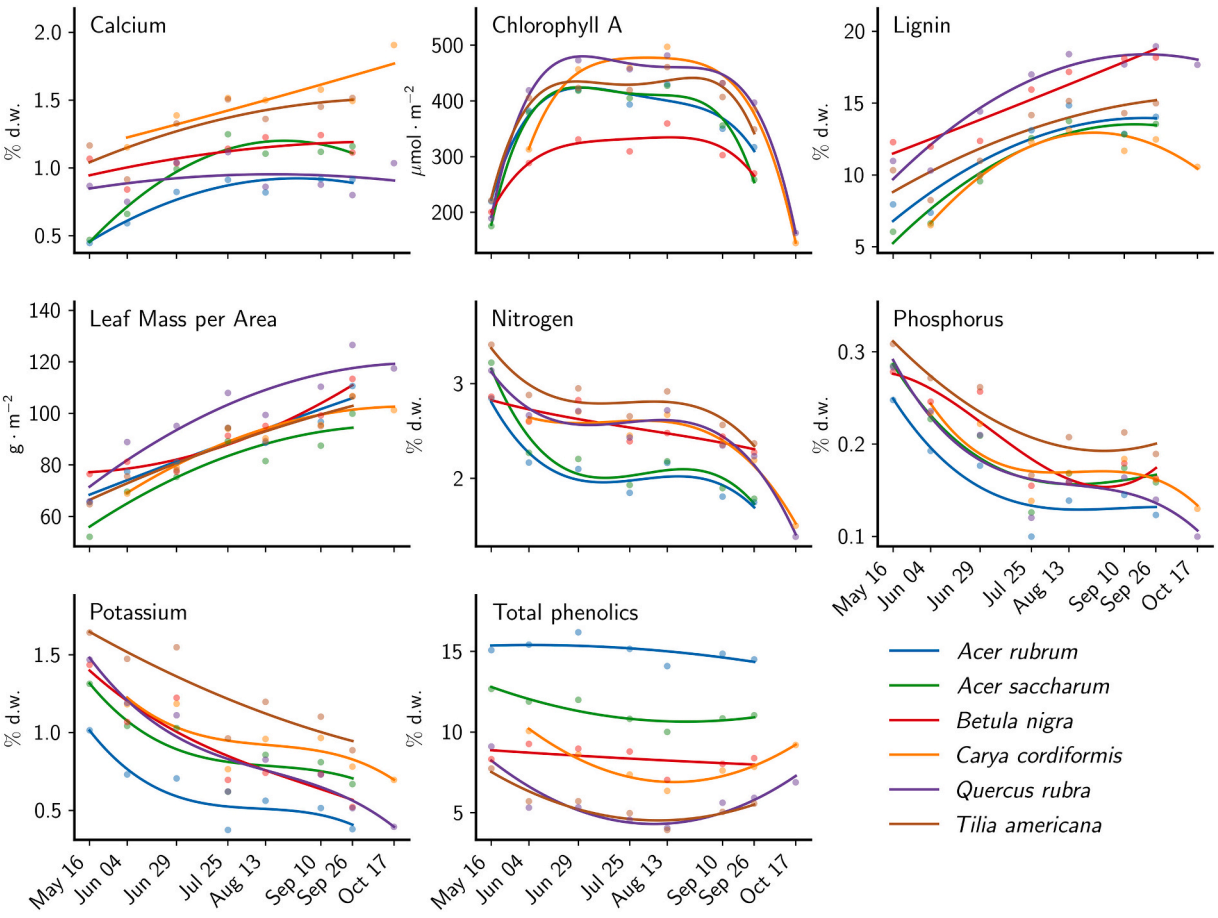

Fig. 6. Seasonal trajectories of traits derived from imaging spectroscopy for five broadleaf species on Blackhawk Island. Trajectories were fit using 2nd (calcium, LMA, lignin, total phenolics), 3rd (nitrogen, phosphorus, potassium) and 4th (chlorophyll A) order polynomials. Sugar and red maple (*Acer saccharum, A. rubrum*), basswood (*T. americana*) and river birch (*B. nigra*) are not shown for October as nearly all trees had dropped all their leaves. Bitternut hickory (*C. cordiformis*) was not shown for May as most trees had not leafed out. (For interpretation of the references to color in this figure legend, the reader is referred to the web version of this article.)

that image-derived estimates of calcium in white oak (*Quercus alba*) were systematically overestimated on May 16 compared to field measurements (image average: 1.58% mass; field average: 0.40% mass). At the time of the May 16 overflight white oak trees had not developed a fully closed canopy (average leaf area on May 16: 8.2 cm^2 vs. June-Oct: 44.5 cm^2) highlighting the importance of considering species specific phenology when interpreting seasonal trait maps. While white oak represents the extreme in our study area, < 20% leaf expansion, field measurements of leaf area indicated that leaf expansion percentages ranged from 35 to 70% on May 16 for all other sampled trees. In some cases, it is likely that traits of the understory vegetation contribute to image-predicted traits in early-season imagery.

4.2. Phenological trends in traits

The trends in mapped chlorophyll content follow expected phenological patterns of green-up and senescence observed from multispectral spaceborne platforms (Melaas et al., 2013; Li et al., 2019). However, with the high spatial resolution of the HySpex airborne sensor, we also detected variation in phenological phenomena among species (Fig. 6). Our maps captured the variability in phenological timing between species, most notably the delayed development of bitternut hickory and early senescence of sugar maple. We also observed lower peak chlorophyll A content in *Betula nigra* and *Acer saccharinum* (not shown in Fig. 6) canopies compared to all other species. On Blackhawk Island, *B. nigra* and *A. saccharinum* are both found growing on sandy soils (Pastor et al., 1982), which are generally low in nutrients including magnesium, a key component of the chlorophyll A molecule (Farhat et al., 2016).

Phenological patterns in total phenolics closely matched those reported in the literature for the same or similar species. Rossiter et al. (1988) and Louis et al. (2009) both observed that phenolic concentrations in *Quercus* species were highest immediately following leaf emergence and stabilized at low levels after full leaf expansion, mirroring the patterns observed in *Quercus* species at Blackhawk Island. High concentrations of phenolics early in the growing season may inhibit herbivory before the development of unpalatable structural compounds like lignin (Lambers and Poorter, 1992). We found that for several non-*Acer* species total phenolics also showed an increase at the end of the growing season, following patterns observed by Schultz et al. (1982) in *Betula alleghanienis*. Similar to our results, Schultz et al. (1982) found that sugar maple foliage reached a maximum level of phenolics early in the growing season and declined through the growing season. While phenolic compounds are generally studied within the context of plant-herbivore interactions, the analytical method we used to measure total phenolics is sensitive to a broad range of phenolic compounds that differ in identity both among species and within a species during a single growing season (Nicol, 1997; Appel et al., 2001). As such, it is difficult to interpret the causation underlying intra-annual patterns or interspecific differences. Beyond their role as defensive compounds against herbivory, phenolics are also associated with photoprotection, nutrient stress, cold acclimation and litter decomposition rates (Dixon and Paiva, 1995; Close and McArthur, 2002; Pennycooke et al., 2005; Hättenschwiler and

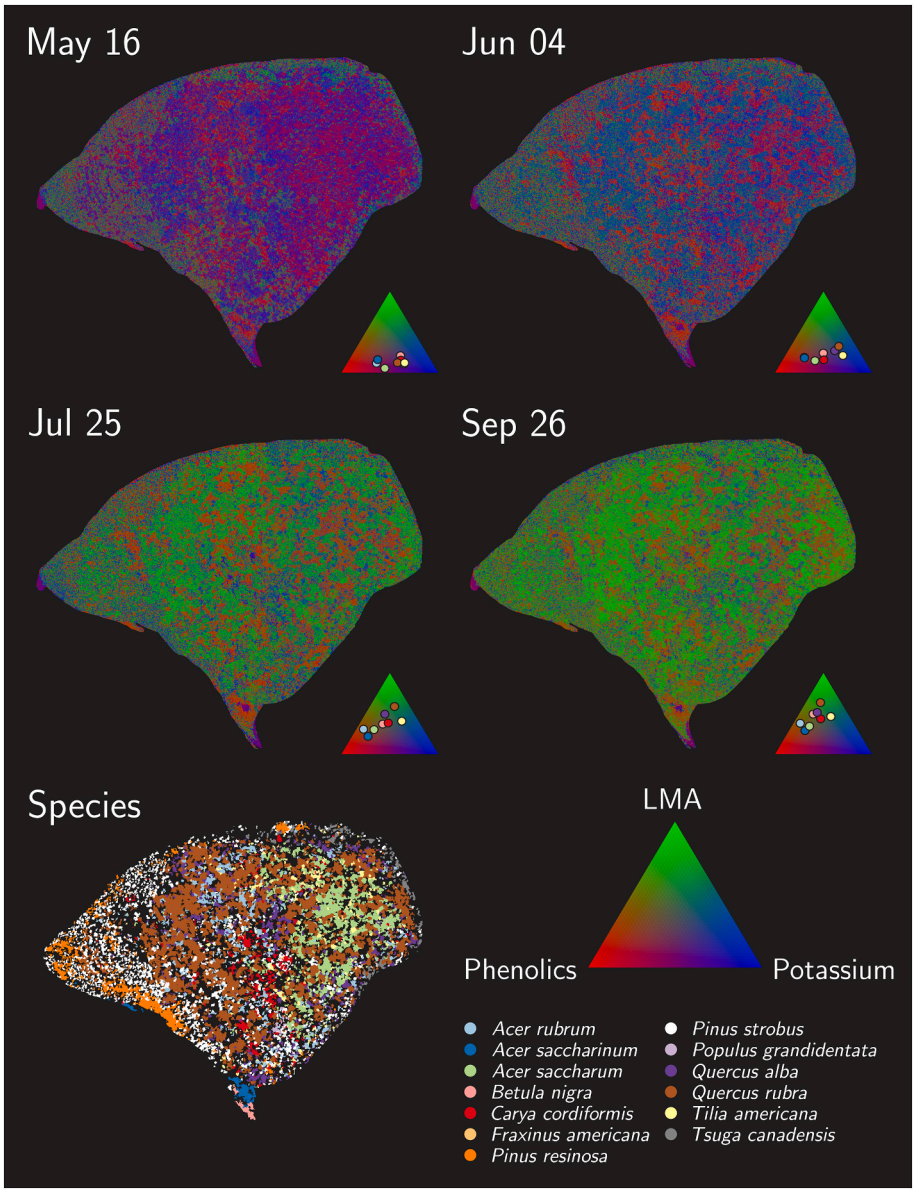

Fig. 7. Top two rows: RGB composite images of total phenolics (red), LMA (green) and potassium (blue) at four time points during the growing season. For each date the species wise averages of the eight most common broadleaf species are shown on the ternary legend. Bottom left: species map, only trees with >30% classification probability are shown, to exclude canopy gaps, shadows and low growing vegetation. (For interpretation of the references to color in this figure legend, the reader is referred to the web version of this article.)

Jørgensen, 2010).

Nutrients related to growth, including nitrogen, potassium and phosphorus, all decreased in concentration during the course of the growing season, as a consequence of dilution by increased content of carbon-rich structural compounds as leaves develop (Chapin, 1980), followed by resorption at the end of the growing season (Killingbeck, 1996). In contrast, calcium, which plays an important role in cell wall formation, increased as the growing season progressed, but is not resorbed due to its low mobility in phloem (Guha and Mitchell, 1966; Zipkin, 1973; Day and Monk, 1977). Similar patterns were observed in lignin and LMA, which increase during the season, reflecting an investment in structural compounds as leaves develop (Groeneveld et al., 1998; Poorter et al., 2009).

While our study site was small, intra-annual maps of traits over larger areas with more significant gradients in soils, topography and climate may provide more insights into drivers of variation in foliar biochemistry than field measurements alone. Such maps would also provide a framework to understand the impacts of phenology on estimates of functional diversity and its contribution to a range of ecological functions (Durán et al., 2019). Moreover, seasonal maps of traits may act as inputs into the next generation of vegetation models that are able to take advantage of rich spatially explicit information provided by imaging spectroscopy beyond basic plant functional types (Berzaghi et al., 2020).

4.3. Implications for broad-scale application

Our maps of foliar traits represent top-of-canopy conditions. Because some traits vary through the canopy as a function of biotic and abiotic variables, these top-of-canopy estimates may not be representative of within or total canopy biochemistry. Others have used measurements of leaf area index (LAI) (Smith et al., 2002; Ollinger et al., 2008) or published foliage distribution data (Singh et al., 2015) to upscale to whole canopy traits, however, these approaches are dependent on a robust relationship between the top-of-canopy reflectance signal and total canopy biochemistry. More recently, coincident lidar and imaging spectroscopy data have been used to estimate full-canopy foliar traits (Chlus et al., 2020; Kamoske et al., 2021). Regardless of scaling technique, developing and validating these full-canopy approaches remains a challenge due to the labor-intensive fieldwork require to collect within-canopy samples.

In this study we focused on broadleaf deciduous species, and

continued work is needed to assess the ability of imaging spectroscopy to characterize seasonal variation across a range of species and ecosystems. For example, needleleaf species also display seasonal variation in canopy biochemistry associated with the development of new needles and remobilization of nutrients into existing foliage (Wyttenbach and Tobler, 1988; Billow et al., 1994). As well, foliar traits can vary significantly in grasslands, for example where the relative dominance of species changes over the course of the growing season such as from C_3 to C_4 and back to C_3 species (Dickinson and Dodd, 1976). Outside of temperate ecosystems, there is also considerable seasonal variability in tropical systems. Species in dry deciduous systems would be expected to show variability in traits related to leaf structure and water conservation (Ishida et al., 2006; Kenzo et al., 2016). Moist tropical systems also exhibit variability, since leaf turnover occurs year-round (Hikosaka, 2005), while seasonality in Mediterranean systems is variable due to climate drivers (Sperlich et al., 2015).

Our work focused on a single growing season, but foliar biochemistry also varies from year-to-year (Mitchell, 1936; Taylor and Parkinson, 1988). Plant phenology is known to be driven by climatic variation, which thus affects allocation of resources at the leaf level (Shen et al., 2011; Liu et al., 2016). For instance, long-term trends of increasing temperatures are associated with earlier spring green-up (Cleland et al., 2007; Dai et al., 2019), for which imaging spectroscopy could provide an approach to document resulting impacts on foliar traits and associated vegetation function. Numerous other factors also alter phenological timing and could be expressed in foliar traits, including biotic forcings, such as herbivory (Lemoine et al., 2017), plant developmental stage and ontogeny (Augspurger and Bartlett, 2003; Grassi et al., 2005). However, our understanding of the patterns and drivers of interannual variation in foliar biochemistry is limited to few species or localized areas, largely due to the challenges of making in situ measurements. Continued long-term imaging with airborne and future spaceborne spectroscopy missions will provide a better understanding of the role of climate, environment and ontogeny in driving intra-annual variability in foliar biochemistry and subsequent impacts on ecological processes.

Our study site had relatively low species diversity (< 15 broadleaf species), whereas highly diverse ecosystems like tropical forests can have hundreds of species in a comparable area (Keil and Chase, 2019). Globally, there are over 300,000 vascular plant species (Christenhusz and Byng, 2016) and over 60,000 tree species (Beech et al., 2017), which has been a strong justification for utilizing a trait- rather than species-based approach to characterizing ecosystems and their function. However, given the diversity of plants on Earth, further investigation is needed into the feasibility of developing global, cross-seasonal predictive models to map foliar traits or, alternatively, whether locally optimized models are more appropriate. Models for some traits like chlorophyll and total phenolics, which have relatively well characterized absorption features, may be well suited for a global model approach. In contrast, traits like calcium, for which the underlying relationship between trait and spectra is ambiguous, may require ecosystem-specific modeling. Despite the low species diversity in our study area, pairwise correlations between both PLSR coefficients and field measured traits were positively correlated with those reported by Chadwick and Asner (2016b) (Pearson $r = 0.76$ and 0.84, respectively, $p < .05$), who used imaging spectroscopy to map canopy traits in Amazonian rainforests, suggesting similar underlying trait and spectral relationships across ecosystems.

4.4. Methodological implications

The choice of predictive algorithm on seasonal trait retrievals also warrants further investigation. We chose PLSR, a data-driven approach, for developing our mapping algorithms. Unlike other empirical methods, like Gaussian process regression (GPR), PLSR does not provide explicit uncertainties. Instead, we used a permutational approach to estimate prediction uncertainties. We found that the magnitudes of the uncertainties were largely a function of whether a given surface/vegetation type was included in our models. For example, canopy gaps, conifers, fields, impervious surfaces and water all had high uncertainties while uncertainties for broadleaf trees were generally uniformly low. Wang et al. (2019) reported similar results in grassland experiment and found that grass plots with conditions not represented in the field data had higher uncertainties. Other data-driven methods have also been used for mapping foliar traits from imaging spectroscopy with comparable levels of accuracy to PLSR, including GPR (Verrelst et al., 2012; Wang et al., 2019) and neural networks (Mutanga and Skidmore, 2004). Radiative transfer models (RTM), like 4SAIL (Verhoef et al., 2007) and INFORM (Atzberger, 2000), provide an alternative method for trait retrieval using a physically based approach to model light transmission as a function of canopy and leaf properties (Schlerf and Atzberger, 2006). RTMs also have been used to estimate traits across the growing season at the leaf level (Gara et al., 2019), however the catalog of biochemical traits retrieved using RTMs is limited to those with well-defined absorbance properties. More recent work has combined RTMs with machine learning (ML) methods to develop a hybrid approach for estimating foliar biochemistry where RTM simulations are used to train ML models (Verrelst et al., 2016; Berger et al., 2020), although RTM-based approaches have not been widely implemented in complex natural vegetation. See Verrelst et al. (2019) for a comprehensive review of modeling techniques for foliar biochemistry retrievals.

Current and future spaceborne imaging spectroscopy missions (ex: DESIS, PRISMA, CHIME, EnMAP and SBG) will provide the opportunity to map seasonal variation in foliar biochemistry on a global scale. These maps will provide spatial context to both inform and complement databases of field measurements (e.g., Kattge et al., 2020) and modeled predictions of global traits (e.g., Butler et al., 2017; Moreno-Martínez et al., 2018; Vallicrosa et al., 2021), while potentially also providing inputs to drive and/or validate earth system models. The lower spatial resolution (20–30 m) pixels of current and planned spaceborne imagers will be composed of species mixes, as well as canopy gaps (possibly with understory vegetation present), shadows and non-vegetated areas in addition to vegetation. In contrast, the high spatial resolution of our imagery allowed us to develop and apply our models on individual trees and mask non vegetated areas. As such, more work is needed to test the impacts of spatial resolution on biochemistry retrievals. Moreover, the presence of multiple species in a single pixel may make interpretation of spatiotemporal patterns in foliar biochemistry and functional diversity challenging.

5. Conclusion

We used imaging spectroscopy to characterize the variation in foliar biochemistry in nine traits across the course of a growing season in a temperate broadleaf deciduous forest. Our method used a single cross-seasonal model to map foliar biochemistry at eight time points from May to October, but we also tested the consequences of using models on dates and species that were withheld from analyses. We demonstrate that seasonal patterns in foliar traits are highly variable, both spatially and temporally, and not all traits follow a consistent pattern of increase and/or decrease whereby mid-season trait values at peak greenness can be considered representative. Thus, the date of image collection can significantly impact inferences made about ecosystem processes. Our research illustrates that when using data-driven methods to map canopy traits, models will generally need to be developed using data representing the full range of values expected to be encountered. Our results demonstrate the potential for future spaceborne imaging spectrometers to map ecologically important seasonal variations in foliar biochemistry.

Data availability

Field data, leaf spectra and canopy spectra can be found in the EcoSIS spectral repository (https://ecosis.org/). Leaf and canopy-level spectral

models can be found in the Ecological Spectral Model Library (https://ecosml.org/). Species and trait maps can be found on the Dryad Data Repository (https://doi.org/10.5061/dryad.4j0zpc8cm).

CRediT authorship contribution statement

Adam Chlus: Conceptualization, Investigation, Formal analysis, Software, Writing – original draft. **Philip A. Townsend:** Conceptualization, Writing – review & editing, Funding acquisition.

Declaration of Competing Interest

The authors declare that they have no known competing financial interests or personal relationships that could have appeared to influence the work reported in this paper.

Acknowledgments

We are grateful to the members of the Townsend lab for their help with fieldwork and sample processing including Abigail Walther, Alex Horvath, Anghad Dhariwal, Ben Spaier, Ben Townsend, Brendan Heberlein, Dewi Radin Umar, Jacob Gold, Josie Mayhew, Raina Eddy and Sam Jaeger. We thank Clayton Kingdon, Erin Wagner, Ittai Herrmann and Nanfeng Liu for their help with image collection and processing. We are also grateful to the pilots and staff at the Wisconsin Department of Natural Resources and Upham Woods for providing operational and logistical support. This research was supported by USDA McIntire-Stennis grants WIS01809 and WIS03008, NSF Macrosystems and Early NEON Science grant 1638720 and NSF ASCEND Biology Integration Institute grant DBI-2021898 to PAT.

Appendix A. Supplementary data

Supplementary data to this article can be found online at https://doi.org/10.1016/j.rse.2022.113023.

References

Adler-Golden, S.M., Matthew, M.W., Bernstein, L.S., Levine, R.Y., Berk, A., Richtsmeier, S.C., Acharya, P.K., Anderson, G.P., Felde, J.W., Gardner, J.A., Hoke, M.L., et al., 1999. Atmospheric correction for shortwave spectral imagery based on MODTRAN4. Imaging Spectrom. In: Descour, M.R., Shen, S.S. (Eds.), Presented at the SPIE's International Symposium on Optical Science, Engineering, and Instrumentation. SPIE, Denver, CO, pp. 61–69.

Ainsworth, E.A., Gillespie, K.M., 2007. Estimation of total phenolic content and other oxidation substrates in plant tissues using Folin–Ciocalteu reagent. Nat. Protoc. 2 (4), 875–877.

Albert, C.H., Thuiller, W., Yoccoz, N.G., Douzet, R., Aubert, S., Lavorel, S., 2010. A multi-trait approach reveals the structure and the relative importance of intra-vs. interspecific variability in plant traits. Funct. Ecol. 24 (6), 1192–1201.

Albert, C.H., Grassein, F., Schurr, F.M., Vieilledent, G., Violle, C., 2011. When and how should intraspecific variability be considered in trait-based plant ecology? Perspect. Plant Ecol. Evol. Syst. 13 (3), 217–225.

Alway, F.J., Maki, T.E., Methley, W.J., 1934. Composition of the leaves of some forest trees. Soil Sci. Soc. Am. J. 15 (2001), 81–84.

Appel, H.M., Govenor, H.L., D'ascenzo, M., Siska, E., Schultz, J.C., 2001. Limitations of Folin assays of foliar phenolics in ecological studies. J. Chem. Ecol. 27 (4), 761–778.

Asner, G.P., Martin, R.E., 2008. Spectral and chemical analysis of tropical forests: scaling from leaf to canopy levels. Remote Sens. Environ. 112 (10), 3958–3970.

Asner, G.P., Martin, R.E., 2011. Canopy phylogenetic, chemical and spectral assembly in a lowland Amazonian forest. New Phytol. 189 (4), 999–1012.

Asner, G.P., Carlson, K.M., Martin, R.E., 2005. Substrate age and precipitation effects on Hawaiian forest canopies from spaceborne imaging spectroscopy. Remote Sens. Environ. 98 (4), 457–467.

Asner, G.P., Martin, R.E., Carranza-Jiménez, L., Sinca, F., Tupayachi, R., Anderson, C.B., Martinez, P., 2014. Functional and biological diversity of foliar spectra in tree canopies throughout the Andes to Amazon region. New Phytol. 204 (1), 127–139.

Asner, G.P., Martin, R.E., Anderson, C.B., Knapp, D.E., 2015. Quantifying forest canopy traits: imaging spectroscopy versus field survey. Remote Sens. Environ. 158, 15–27.

Atzberger, C., 2000. Development of an invertible forest reflectance model: The INFOR-model. In: Proceedings of the 20th EARSeL Symposium. CRC Press/Balkema.

Augspurger, C.K., Bartlett, E.A., 2003. Differences in leaf phenology between juvenile and adult trees in a temperate deciduous forest. Tree Physiol. 23 (8), 517–525.

Beech, E., Rivers, M., Oldfield, S., Smith, P.P., 2017. GlobalTreeSearch: the first complete global database of tree species and country distributions. J. Sustain. For. 36 (5), 454–489.

Berger, K., Verrelst, J., Féret, J.B., Hank, T., Wocher, M., Mauser, W., Camps-Valls, G., 2020. Retrieval of aboveground crop nitrogen content with a hybrid machine learning method. Int. J. Appl. Earth Obs. Geoinf. 92, 102174.

Berzaghi, F., Wright, I.J., Kramer, K., Oddou-Muratorio, S., Bohn, F.J., Reyer, C.P.O., Sabaté, S., Sanders, T.G.M., Hartig, F., 2020. Towards a new generation of trait-flexible vegetation models. Trends Ecol. Evol. 35 (3), 191–205. https://doi.org/10.1016/j.tree.2019.11.006.

Billow, C., Matson, P., Yoder, B., 1994. Seasonal biochemical changes in coniferous forest canopies and their response to fertilization. Tree Physiol. 14 (6), 563–574.

Bunting, P., Clewley, D., Lucas, R.M., Gillingham, S., 2014. The remote sensing and GIS software library (RSGISLib). Comput. Geosci. 62, 216–226.

Butler, E.E., Datta, A., Flores-Moreno, H., Chen, M., Wythers, K.R., Fazayeli, F., Banerjee, A., Atkin, O.K., Kattge, J., Amiaud, B., Blonder, B., Boenisch, G., Bond-Lamberty, B., Brown, K.A., Byun, C., Campetella, G., Cerabolini, B.E., Cornelissen, J. H., Craine, J.M., Reich, P.B., 2017. Mapping local and global variability in plant trait distributions. Proc. Natl. Acad. Sci. 114 (51) https://doi.org/10.1073/pnas.1708984114.

Carrere, V., Conel, J.E., 1993. Recovery of atmospheric water vapor total column abundance from imaging spectrometer data around 940 nm—sensitivity analysis and application to airborne visible/infrared imaging spectrometer (AVIRIS) data. Remote Sens. Environ. 44 (2–3), 179–204.

Chadwick, K.D., Asner, G.P., 2016a. Tropical soil nutrient distributions determined by biotic and hillslope processes. Biogeochemistry 127 (2–3), 273–289.

Chadwick, K.D., Asner, G.P., 2016b. Organismic-scale remote sensing of canopy foliar traits in lowland tropical forests. Remote Sens. 8 (2), 87.

Chadwick, K.D., Asner, G.P., 2018. Landscape evolution and nutrient rejuvenation reflected in Amazon forest canopy chemistry. Ecol. Lett. 21 (7), 978–988.

Chandler, R.F., 1939. The Calcium Content of the Foliage of Forest Trees. Cornell University Agriculture Experiment Station, Memo, p. 228.

Chandler Jr., R.F., 1941. Amount and mineral nutrient content of freshly fallen leaf litter in the hardwood forests of Central New York. J. Am. Soc. Agron. 33 (10).

Chapin III, F.S., 1980. The mineral nutrition of wild plants. Annu. Rev. Ecol. Syst. 11 (1), 233–260.

Cheng, T., Rivard, B., Sánchez-Azofeifa, A.G., Féret, J.B., Jacquemoud, S., Ustin, S.L., 2014. Deriving leaf mass per area (LMA) from foliar reflectance across a variety of plant species using continuous wavelet analysis. ISPRS J. Photogramm. Remote Sens. 87, 28–38.

Chlus, A., Kruger, E.L., Townsend, P.A., 2020. Mapping three-dimensional variation in leaf mass per area with imaging spectroscopy and lidar in a temperate broadleaf forest. Remote Sens. Environ. 250, 112043.

Christenhusz, M.J., Byng, J.W., 2016. The number of known plants species in the world and its annual increase. Phytotaxa 261 (3), 201–217.

Cleland, E.E., Chuine, I., Menzel, A., Mooney, H.A., Schwartz, M.D., 2007. Shifting plant phenology in response to global change. Trends Ecol. Evol. 22 (7), 357–365.

Close, D.C., McArthur, C., 2002. Rethinking the role of many plant phenolics–protection from photodamage not herbivores? Oikos 99 (1), 166–172.

Côté, B., Fyles, J.W., 1994. Nutrient concentration and acid–base status of leaf litter of tree species characteristic of the hardwood forest of southern Quebec. Can. J. For. Res. 24 (1), 192–196.

Couture, J.J., Meehan, T.D., Lindroth, R.L., 2012. Atmospheric change alters foliar quality of host trees and performance of two outbreak insect species. Oecologia 168 (3), 863–876.

Couture, J.J., Singh, A., Rubert-Nason, K.F., Serbin, S.P., Lindroth, R.L., Townsend, P.A., 2016. Spectroscopic determination of ecologically relevant plant secondary metabolites. Methods Ecol. Evol. 7 (11), 1402–1412.

Curran, P.J., 1989. Remote sensing of foliar chemistry. Remote Sens. Environ. 30 (3), 271–278.

Dai, W., Jin, H., Zhang, Y., Liu, T., Zhou, Z., 2019. Detecting temporal changes in the temperature sensitivity of spring phenology with global warming: application of machine learning in phenological model. Agric. For. Meteorol. 279, 107702.

Day Jr., F.P., Monk, C.D., 1977. Seasonal nutrient dynamics in the vegetation on a southern Appalachian watershed. Am. J. Bot. 64 (9), 1126–1139.

de Bello, F., Lavorel, S., Díaz, S., Harrington, R., Cornelissen, J.H., Bardgett, R.D., Berg, M.P., Cipriotti, P., Feld, C.K., Hering, D., Martins da Silva, P., Potts, S.G., Sandin, L., Sousa, J.P., Storkey, J., Wardle, D.A., Harrison, P.A., 2010. Towards an assessment of multiple ecosystem processes and services via functional traits. Biodivers. Conserv. 19 (10), 2873–2893.

Díaz, S., Kattge, J., Cornelissen, J.H., Wright, I.J., Lavorel, S., Dray, S., Reu, B., Kleyer, M., Wirth, C., Colin Prentice, I., Garnier, E., Bönisch, G., Westoby, M., Poorter, H., Reich, P.B., Moles, A.T., Dickie, J., Gillison, A.N., Zanne, A.E., Gorné, L. D., 2015. The global spectrum of plant form and function. Nature 529 (7585), 167–171.

Dickinson, C.E., Dodd, J.L., 1976. Phenological pattern in the shortgrass prairie. Am. Midl. Nat. 367–378.

Dixon, R.A., Paiva, N.L., 1995. Stress-induced phenylpropanoid metabolism. Plant Cell 7 (7), 1085.

Dong, N., Prentice, I.C., Wright, I.J., Evans, B.J., Togashi, H.F., Caddy-Retalic, S., McInerney, F.A., Sparrow, B., Leitch, E., Lowe, A.J., 2020. Components of leaf-trait variation along environmental gradients. New Phytol. 228 (1), 82–94. https://doi.org/10.1111/nph.16558.

Duchemin, B., Goubier, J., Courrier, G., 1999. Monitoring phenological key stages and cycle duration of temperate deciduous forest ecosystems with NOAA/AVHRR data. Remote Sens. Environ. 67 (1), 68–82.

Durán, S.M., Martin, R.E., Díaz, S., Maitner, B.S., Malhi, Y., Salinas, N., Shenkin, A., Silman, M.R., Wieczynski, D.J., Asner, G.P., Bentley, L.P., Savage, V.M., Enquist, B. J., 2019. Informing trait-based ecology by assessing remotely sensed functional diversity across a broad tropical temperature gradient. Sci. Adv. 5 (12).

Emde, C., Buras-Schnell, R., Kylling, A., Mayer, B., Gasteiger, J., Hamann, U., Kylling, J., Richter, B., Pause, C., Dowling, T., Bugliaro, L., 2016. The libRadtran software package for radiative transfer calculations (version 2.0.1). Geosci. Model Dev. 9 (5), 1647–1672.

Farhat, N., Elkhouni, A., Zorrig, W., Smaoui, A., Abdelly, C., Rabhi, M., 2016. Effects of magnesium deficiency on photosynthesis and carbohydrate partitioning. Acta Physiol. Plant. 38 (6), 145.

Feilhauer, H., Asner, G.P., Martin, R.E., Schmidtlein, S., 2010. Brightness-normalized partial least squares regression for hyperspectral data. J. Quant. Spectrosc. Radiat. Transf. 111 (12–13), 1947–1957.

Flower, C.E., 2007. Seasonal Carbohydrate Allocation in Big Tooth Aspen (*Populus grandidentata* Michx.) and Northern Red Oak (*Quercus rubra* L.) from Northern Lower Michigan. Doctoral dissertation. The Ohio State University.

Gao, F., Masek, J.G., Wolfe, R.E., 2009. Automated registration and orthorectification package for Landsat and Landsat-like data processing. J. Appl. Remote. Sens. 3 (1), 033515.

Gara, T.W., Darvishzadeh, R., Skidmore, A.K., Wang, T., Heurich, M., 2019. Evaluating the performance of PROSPECT in the retrieval of leaf traits across canopy throughout the growing season. Int. J. Appl. Earth Obs. Geoinf. 83, 101919.

Gavlak, R., Horneck, D., Miller, R.O., Kotuby-Amacher, J., 2003. Soil, Plant and Water Reference Methods for the Western Region. WCC-103 Publication, Fort Collins, CO.

Gitelson, A.A., Merzlyak, M.N., Lichtenthaler, H.K., 1996. Detection of red edge position and chlorophyll content by reflectance measurements near 700 nm. J. Plant Physiol. 148 (3–4), 501–508.

Grassi, G., Vicinelli, E., Ponti, F., Cantoni, L., Magnani, F., 2005. Seasonal and interannual variability of photosynthetic capacity in relation to leaf nitrogen in a deciduous forest plantation in northern Italy. Tree Physiol. 25 (3), 349–360.

Groeneveld, H.W., Bergkotte, M., Lambers, H., 1998. Leaf growth in the fast-growing Holcus lanatus and the slow-growing Deschampsia flexuosa: tissue maturation. J. Exp. Bot. 1509–1517.

Guanter, L., Segl, K., Sang, B., Alonso, L., Kaufmann, H., Moreno, J., 2009. Scene-based spectral calibration assessment of high spectral resolution imaging spectrometers. Opt. Express 17 (14), 11594–11606.

Guha, M.M., Mitchell, R.L., 1966. The trace and major element composition of the leaves of some deciduous trees. Plant Soil 24 (1), 90–112.

Hättenschwiler, S., Jørgensen, H.B., 2010. Carbon quality rather than stoichiometry controls litter decomposition in a tropical rain forest. J. Ecol. 98 (4), 754–763.

Hikosaka, K., 2005. Leaf canopy as a dynamic system: ecophysiology and optimality in leaf turnover. Ann. Bot. 95 (3), 521–533.

Insley, H., Boswell, R.C., Gardiner, J.B.H., 1981. Foliar macronutrients (N, P, K, Ca and Mg) in lime (Tilia spp.). Plant Soil 61 (3), 391–401.

Ishida, A., Diloksumpun, S., Ladpala, P., Staporn, D., Panuthai, S., Gamo, M., Yazaki, K., Ishizuka, M., Puangchit, L., 2006. Contrasting seasonal leaf habits of canopy trees between tropical dry-deciduous and evergreen forests in Thailand. Tree Physiol. 26 (5), 643–656. https://doi.org/10.1093/treephys/26.5.643.

Ito, A., Muraoka, H., Koizumi, H., Saigusa, N., Murayama, S., Yamamoto, S., 2006. Seasonal variation in leaf properties and ecosystem carbon budget in a cool-temperate deciduous broad-leaved forest: simulation analysis at Takayama site, Japan. Ecol. Res. 21 (1), 137–149.

Kamoske, A.G., Dahlin, K.M., Serbin, S.P., Stark, S.C., 2021. Leaf traits and canopy structure together explain canopy functional diversity: an airborne remote sensing approach. Ecol. Appl. 31 (2), e02230.

Kattge, J., Bönisch, G., Díaz, S., Lavorel, S., Prentice, I.C., Leadley, P., Tautenhahn, S., Werner, G.D., Aakala, T., Abedi, M., Acosta, A.T., Adamidis, G.C., Adamson, K., Aiba, M., Albert, C.H., Alcántara, J.M., Alcázar, C., Aleixo, I., Ali, H., Wirth, C., 2020. Try plant trait database – enhanced coverage and open access. Glob. Chang. Biol. 26 (1), 119–188. https://doi.org/10.1111/gcb.14904.

Keil, P., Chase, J.M., 2019. Global patterns and drivers of tree diversity integrated across a continuum of spatial grains. Nat. Ecol. Evol. 3 (3), 390–399.

Kenzo, T., Iida, S.I., Shimizu, T., Tamai, K., Kabeya, N., Shimizu, A., Chann, S., 2016. Seasonal and height-related changes in leaf morphological and photosynthetic traits of two dipterocarp species in a dry deciduous forest in Cambodia. Plant Ecol. Divers. 9 (5–6), 505–520.

Killingbeck, K.T., 1996. Nutrients in senesced leaves: keys to the search for potential resorption and resorption proficiency. Ecology 77 (6), 1716–1727.

Kim, G., Kim, D.Y., Kim, G.H., Cho, B.K., 2013. Applications of discrete wavelet analysis for predicting internal quality of cherry tomatoes using VIS/NIR spectroscopy. J. Biosyst. Eng. 38 (1), 48–54.

Kokaly, R.F., Skidmore, A.K., 2015. Plant phenolics and absorption features in vegetation reflectance spectra near 1.66 μm. Int. J. Appl. Earth Obs. Geoinf. 43, 55–83.

Lambers, H.A.N.S., Poorter, H., 1992. Inherent variation in growth rate between higher plants: a search for physiological causes and ecological consequences. In: Advances in Ecological Research, vol. 23. Academic Press, pp. 187–261.

Lemoine, N.P., Doublet, D., Salminen, J.P., Burkepile, D.E., Parker, J.D., 2017. Responses of plant phenology, growth, defense, and reproduction to interactive effects of warming and insect herbivory. Ecology 98 (7), 1817–1828.

Li, X., Zhou, Y., Meng, L., Asrar, G.R., Lu, C., Wu, Q., 2019. A dataset of 30 m annual vegetation phenology indicators (1985–2015) in urban areas of the conterminous United States. Earth Syst.Sci. Data 11, 881–894.

Liu, Q., Fu, Y.H., Zeng, Z., Huang, M., Li, X., Piao, S., 2016. Temperature, precipitation, and insolation effects on autumn vegetation phenology in temperate China. Glob. Chang. Biol. 22 (2), 644–655.

Louis, J., Meyer, S., Maunoury-Danger, F., Fresneau, C., Meudec, E., Cerovic, Z.G., 2009. Seasonal changes in optically assessed epidermal phenolic compounds and chlorophyll contents in leaves of sessile oak (Quercus petraea): towards signatures of phenological stage. Funct. Plant Biol. 36 (8), 732–741.

Martin, Mary E., Aber, John D., 1997. High spectral resolution remote sensing of forest canopy lignin, nitrogen, and ecosystem processes. Ecol. Appl. 7 (2), 431–443.

Martin, R.E., Chadwick, K.D., Brodrick, P.G., Carranza-Jimenez, L., Vaughn, N.R., Asner, G.P., 2018. An approach for foliar trait retrieval from airborne imaging spectroscopy of tropical forests. Remote Sens. 10 (2), 199.

Matson, P., Johnson, L., Billow, C., Miller, J., Pu, R., 1994. Seasonal patterns and remote spectral estimation of canopy chemistry across the Oregon transect. Ecol. Appl. 4 (2), 280–298.

McHargue, J.S., Roy, W.R., 1932. Mineral and nitrogen content of the leaves of some forest trees at different times in the growing season. Bot. Gaz. 94 (2), 381–393.

McLaughlin, S.B., McConathy, R.K., Barnes, R.L., Edwards, N.T., 1980. Seasonal changes in energy allocation by white oak (Quercus alba). Can. J. For. Res. 10 (3), 379–388.

Meireles, J.E., Cavender-Bares, J., Townsend, P.A., Ustin, S., Gamon, J.A., Schweiger, A. K., Schaepman, M.E., Asner, G.P., Martin, R.E., Singh, A., Schrodt, F., Chlus, A., O'Meara, B.C., 2020. Leaf reflectance spectra capture the evolutionary history of seed plants. New Phytol. 228 (2), 485–493.

Melaas, E.K., Friedl, M.A., Zhu, Z., 2013. Detecting interannual variation in deciduous broadleaf forest phenology using Landsat TM/ETM+ data. Remote Sens. Environ. 132, 176–185.

Messier, J., McGill, B.J., Lechowicz, M.J., 2010. How do traits vary across ecological scales? A case for trait-based ecology. Ecol. Lett. 13 (7), 838–848.

Messier, J., McGill, B.J., Enquist, B.J., Lechowicz, M.J., 2017. Trait variation and integration across scales: is the leaf economic spectrum present at local scales? Ecography 40 (6), 685–697.

Mitchell, H.L., 1936. Trends in the nitrogen, phosphorus, potassium and calcium content of the leaves of some forest trees during the growing season. Black Rock Forest Pap. 1 (6), 30–44.

Moreno-Martínez, Á., Camps-Valls, G., Kattge, J., Robinson, N., Reichstein, M., van Bodegom, P., Kramer, K., Cornelissen, J.H., Reich, P., Bahn, M., Niinemets, Ü., Peñuelas, J., Craine, J.M., Cerabolini, B.E.L., Minden, V., Laughlin, D.C., Sack, L., Allred, B., Baraloto, C., Running, S.W., 2018. A methodology to derive global maps of leaf traits using remote sensing and climate data. Remote Sens. Environ. 218, 69–88.

Mutanga, O., Skidmore, A.K., 2004. Integrating imaging spectroscopy and neural networks to map grass quality in the Kruger National Park, South Africa. Remote Sens. Environ. 90 (1), 104–115.

Nicol, R.W., 1997. The Activity of the Phytochemical Defenses of Red Maple (*Acer rubrum* L.) and Sugar Maple (*Acer saccharum* Marsh.) against the Forest Tent Caterpillar (*Malacosoma disstria* Huebner). Masters Thesis. University of Ottawa (Canada).

Noda, H.M., Muraoka, H., Nasahara, K.N., Saigusa, N., Murayama, S., Koizumi, H., 2015. Phenology of leaf morphological, photosynthetic, and nitrogen use characteristics of canopy trees in a cool-temperate deciduous broadleaf forest at Takayama, Central Japan. Ecol. Res. 30 (2), 247–266.

Nunes, M., Davey, M., Coomes, D., 2017. On the challenges of using field spectroscopy to measure the impact of soil type on leaf traits. Biogeosciences 14 (13), 3371–3385.

Ollinger, S.V., Richardson, A.D., Martin, M.E., Hollinger, D.Y., Frolking, S.E., Reich, P.B., Schmid, H.P., 2008. Canopy nitrogen, carbon assimilation, and albedo in temperate and boreal forests: functional relations and potential climate feedbacks. Proc. Natl. Acad. Sci. 105 (49), 19336–19341.

Osborne, B.G., Fearn, T., Hindle, P.H., 1993. Practical NIR Spectroscopy with Applications in Food and Beverage Analysis. Longman Scientific and Technical.

Pastor, J., Aber, J.D., McClaugherty, C.A., Melillo, J.M., 1982. Geology, soils and vegetation of Blackhawk Island, Wisconsin. Am. Midl. Nat. 266–277.

Pastor, J., Aber, J.D., McClaugherty, C.A., Melillo, J.M., 1984. Aboveground production and N and P cycling along a nitrogen mineralization gradient on Blackhawk Island, Wisconsin. Ecology 65 (1), 256–268.

Pedregosa, F., Varoquaux, G., Gramfort, A., Michel, V., Thirion, B., Grisel, O., Blondel, M., Prettenhofer, P., Weiss, R., Dubourg, V., Vanderplas, J., Passos, A., Cournapeau, D., Brucher, M., Perrot, M., Duchesnay, E., 2011. Scikit-learn: machine learning in Python. J. Mach. Learn. Res. 12, 2825–2830.

Pennycooke, J.C., Cox, S., Stushnoff, C., 2005. Relationship of cold acclimation, total phenolic content and antioxidant capacity with chilling tolerance in petunia (Petunia× hybrida). Environ. Exp. Bot. 53 (2), 225–232.

Poorter, H., Niinemets, Ü., Poorter, L., Wright, I.J., Villar, R., 2009. Causes and consequences of variation in leaf mass per area (LMA): a meta-analysis. New Phytol. 182 (3), 565–588.

Reich, P.B., Walters, M.B., Ellsworth, D.S., 1991. Leaf age and season influence the relationships between leaf nitrogen, leaf mass per area and photosynthesis in maple and oak trees. Plant Cell Environ. 14 (3), 251–259.

Reichstein, M., Bahn, M., Mahecha, M.D., Kattge, J., Baldocchi, D.D., 2014. Linking plant and ecosystem functional biogeography. Proc. Natl. Acad. Sci. 111 (38), 13697–13702.

Rossiter, M., Schultz, J.C., Baldwin, I.T., 1988. Relationships among defoliation, red oak phenolics, and gypsy moth growth and reproduction. Ecology 69 (1), 267–277.

Saeki, I., Dick, C.W., Barnes, B.V., Murakami, N., 2011. Comparative phylogeography of red maple (Acer rubrum L.) and silver maple (Acer saccharinum L.): impacts of habitat specialization, hybridization and glacial history. J. Biogeogr. 38 (5), 992–1005.

Salminen, J.P., Roslin, T., Karonen, M., Sinkkonen, J., Pihlaja, K., Pulkkinen, P., 2004. Seasonal variation in the content of hydrolyzable tannins, flavonoid glycosides, and proanthocyanidins in oak leaves. J. Chem. Ecol. 30 (9), 1693–1711.

Sampson, A.W., Samisch, R., 1935. Growth and seasonal changes in composition of oak leaves. Plant Physiol. 10 (4), 739.
Sanches, I.D., Tuohy, M.P., Hedley, M.J., Mackay, A.D., 2013. Seasonal prediction of in situ pasture macronutrients in New Zealand pastoral systems using hyperspectral data. Int. J. Remote Sens. 34 (1), 276–302.
Sanger, J.E., 1971. Quantitative investigations of leaf pigments from their inception in buds through autumn coloration to decomposition in falling leaves. Ecology 52 (6), 1075–1089.
Schertz, F.M., 1929. Seasonal variation of the chloroplast pigments in several plants on the mall at Washington, D. C. Plant Physiol. 4 (1), 135.
Schläpfer, D., Richter, R., Feingersh, T., 2014. Operational BRDF effects correction for wide-field-of-view optical scanners (BREFCOR). IEEE Trans. Geosci. Remote Sens. 53 (4), 1855–1864.
Schlerf, M., Atzberger, C., 2006. Inversion of a forest reflectance model to estimate structural canopy variables from hyperspectral remote sensing data. Remote Sens. Environ. 100 (3), 281–294.
Schultz, J.C., Nothnagle, P.J., Baldwin, I.T., 1982. Seasonal and individual variation in leaf quality of two northern hardwoods tree species. Am. J. Bot. 69 (5), 753–759.
Schweiger, A.K., Cavender-Bares, J., Townsend, P.A., Hobbie, S.E., Madritch, M.D., Wang, R., Tilman, D., Gamon, J.A., 2018. Plant spectral diversity integrates functional and phylogenetic components of biodiversity and predicts ecosystem function. Nat. Ecol. Evol. 2 (6), 976–982.
Serbin, S.P., Singh, A., McNeil, B.E., Kingdon, C.C., Townsend, P.A., 2014. Spectroscopic determination of leaf morphological and biochemical traits for northern temperate and boreal tree species. Ecol. Appl. 24 (7), 1651–1669.
Serbin, S.P., Wu, J., Ely, K.S., Kruger, E.L., Townsend, P.A., Meng, R., Rogers, A., 2019. From the Arctic to the tropics: multibiome prediction of leaf mass per area using leaf reflectance. New Phytol. 224 (4), 1557–1568.
Shen, M., Tang, Y., Chen, J., Zhu, X., Zheng, Y., 2011. Influences of temperature and precipitation before the growing season on spring phenology in grasslands of the central and eastern Qinghai-Tibetan Plateau. Agric. For. Meteorol. 151 (12), 1711–1722.
Shenk, J.S., Westerhaus, M.O., Hoover, M.R., 1979. Analysis of forages by infrared reflectance. J. Dairy Sci. 62 (5), 807–812.
Shepherd, J.D., Bunting, P., Dymond, J.R., 2019. Operational large-scale segmentation of imagery based on iterative elimination. Remote Sens. 11 (6), 658.
Singh, A., Serbin, S.P., McNeil, B.E., Kingdon, C.C., Townsend, P.A., 2015. Imaging spectroscopy algorithms for mapping canopy foliar chemical and morphological traits and their uncertainties. Ecol. Appl. 25 (8), 2180–2197.
Smith, M.L., Ollinger, S.V., Martin, M.E., Aber, J.D., Hallett, R.A., Goodale, C.L., 2002. Direct estimation of aboveground forest productivity through hyperspectral remote sensing of canopy nitrogen. Ecol. Appl. 12 (5), 1286–1302.
Sperlich, D., Chang, C.T., Peñuelas, J., Gracia, C., Sabaté, S., 2015. Seasonal variability of foliar photosynthetic and morphological traits and drought impacts in a Mediterranean mixed forest. Tree Physiol. 35 (5), 501–520.
Swinfield, T., Both, S., Riutta, T., Bongalov, B., Elias, D., Majalap-Lee, N., Ostle, N., Svátek, M., Kvasnica, J., Milodowski, D., Jucker, T., Ewers, R.M., Zhang, Y., Johnson, D., Teh, Y.A., Burslem, D.F., Malhi, Y., Coomes, D., 2019. Imaging spectroscopy reveals the effects of topography and logging on the leaf chemistry of Tropical Forest canopy trees. Glob. Chang. Biol. 26 (2), 989–1002.
Taylor, B.R., Parkinson, D., 1988. Annual differences in quality of leaf litter of aspen (Populus tremuloides) affecting rates of decomposition. Can. J. Bot. 66 (10), 1940–1947.
Thompson, D.R., Gao, B.C., Green, R.O., Roberts, D.A., Dennison, P.E., Lundeen, S.R., 2015. Atmospheric correction for global mapping spectroscopy: ATREM advances for the HyspIRI preparatory campaign. Remote Sens. Environ. 167, 64–77.
Thompson, D.R., Natraj, V., Green, R.O., Helmlinger, M.C., Gao, B.C., Eastwood, M.L., 2018. Optimal estimation for imaging spectrometer atmospheric correction. Remote Sens. Environ. 216, 355–373.
Turner, J., Dice, S.F., Cole, D.W., Gessel, S.P., 1977. Variation of Nutrients in Forest Tree Foliage: A Review. Technical Report. 32. University of Washington.
Vallicrosa, H., Sardans, J., Maspons, J., Zuccarini, P., Marcos, Fernández-Martínez, Bauters, M., Goll, D.S., Ciais, P., Obersteiner, M., Janssens, I.A., Peñuelas, J., 2021. Global maps and factors driving forest foliar elemental composition: the importance of evolutionary history. New Phytol. 233, 169–181.
Verhoef, W., Jia, L., Xiao, Q., Su, Z., 2007. Unified optical-thermal four-stream radiative transfer theory for homogeneous vegetation canopies. IEEE Trans. Geosci. Remote Sens. 45 (6), 1808–1822.
Verrelst, J., Alonso, L., Caicedo, J.P.R., Moreno, J., Camps-Valls, G., 2012. Gaussian process retrieval of chlorophyll content from imaging spectroscopy data. IEEE J. Sel. Top. Appl. Earth Obs. Remote Sens. 6 (2), 867–874.
Verrelst, J., Dethier, S., Rivera, J.P., Munoz-Mari, J., Camps-Valls, G., Moreno, J., 2016. Active learning methods for efficient hybrid biophysical variable retrieval. IEEE Geosci. Remote Sens. Lett. 13 (7), 1012–1016.
Verrelst, J., Malenovský, Z., Van der Tol, C., Camps-Valls, G., Gastellu-Etchegorry, J.P., Lewis, P., North, P., Moreno, J., 2019. Quantifying vegetation biophysical variables from imaging spectroscopy data: a review on retrieval methods. Surv. Geophys. 40 (3), 589–629.
Wang, Z., Townsend, P.A., Schweiger, A.K., Couture, J.J., Singh, A., Hobbie, S.E., Cavender-Bares, J., 2019. Mapping foliar functional traits and their uncertainties across three years in a grassland experiment. Remote Sens. Environ. 221, 405–416.
Wang, Z., Chlus, A., Geygan, R., Ye, Z., Zheng, T., Singh, A., Couture, J.J., Cavender-Bares, J., Kruger, E.L., Townsend, P.A., 2020. Foliar functional traits from imaging spectroscopy across biomes in eastern North America. New Phytol. 228 (2), 494–511. https://doi.org/10.1111/nph.16711.
Wessman, C.A., Aber, J.D., Peterson, D.L., Melillo, J.M., 1988. Remote sensing of canopy chemistry and nitrogen cycling in temperate forest ecosystems. Nature 335 (6186), 154–156.
Weyermann, J., Damm, A., Kneubühler, M., Schaepman, M.E., 2013. Correction of reflectance anisotropy effects of vegetation on airborne spectroscopy data and derived products. IEEE Trans. Geosci. Remote Sens. 52 (1), 616–627.
Workman Jr., J., Weyer, L., 2008. Practical Guide to Interpretive Near-Infrared Spectroscopy. CRC Press.
Wu, C., Niu, Z., Tang, Q., Huang, W., Rivard, B., Feng, J., 2009. Remote estimation of gross primary production in wheat using chlorophyll-related vegetation indices. Agric. For. Meteorol. 149 (6–7), 1015–1021.
Wyttenbach, A., Tobler, L., 1988. The seasonal variation of 20 elements in 1st and 2nd year needles of Norway spruce, Picea abies (L.) Karst. Trees 2 (1), 52–64.
Yang, X., Tang, J., Mustard, J.F., Wu, J., Zhao, K., Serbin, S., Lee, J.E., 2016. Seasonal variability of multiple leaf traits captured by leaf spectroscopy at two temperate deciduous forests. Remote Sens. Environ. 179, 1–12.
Zehnder, C.B., Stodola, K.W., Joyce, B.L., Egetter, D., Cooper, R.J., Hunter, M.D., 2009. Elevational and seasonal variation in the foliar quality and arthropod community of Acer pensylvanicum. Environ. Entomol. 38 (4), 1161–1167.
Zipkin, I. (Ed.), 1973. Biological Mineralization. Krieger Publishing Company.